GREEN SYNTHESIS AND CHARACTERIZATION OF COPPER(II) OXIDE NANOPARTICLES DERIVED FROM LEMON (*Citrus limon*) PEEL EXTRACT FOR THE PHOTOCATALYTIC DEGRADATION OF PALM OIL MILL EFFLUENT (POME)

By

TAN LEE XIAN

A project report submitted to the Department of Chemical Science

Faculty of Science

Universiti Tunku Abdul Rahman

in partial fulfilment of the requirements for the degree of

Bachelor of Science (Hons) Chemistry

May 2022

ABSTRACT

GREEN SYNTHESIS AND CHARACTERIZATION OF COPPER(II) OXIDE NANOPARTICLES DERIVED FROM LEMON (*Citrus limon*) PEEL EXTRACT FOR THE PHOTOCATALYTIC DEGRADATION OF PALM OIL MILL EFFLUENT (POME)

Tan Lee Xian

The properties of matter at nanoscale are significantly different from their macroscopic bulk properties. Metal nanoparticles have been applied for various applications, such as biosensor, controlled drug delivery, antimicrobial agent and photocatalysts for wastewater treatment. Nanoparticles able to degrade pollutants under ultraviolet (UV) light, is one the favorable method for wastewater treatment. Nowadays, there are various physical and chemical methods have been used to synthesize nanoparticles. However, there are a lot of serious threats to the environment by using these methods due to the usage of toxic chemicals and solvents, consumption of high energy, high cost, and tedious procedure. Therefore, there is a need for "green synthesis" of nanoparticles due to its simplicity, nontoxicity, nonexpensive, energy efficiency, and

environmentally friendliness. In this study, copper(II) oxide nanoparticles, CuO NPs were synthesized using lemon (*Citrus limon*) peel extract (LPE) as reducing and stabilizing agent, and copper(II) nitrate trihydrate salt as precursor. LPE was prepared with deionized water by heating 20 minutes and filtering twice, and copper(II) nitrate trihydrate was added into LPE with continuous heating and stirring until dark green paste is obtained. Then, dark green paste was calcinated in furnace at 450 ℃ for 2 hours. Green synthesized CuO NPs were characterized by UV-visible (UV-vis) spectroscopy, fourier transform infrared spectroscopy (FTIR), energy dispersive X-ray (EDX) spectroscopy, X-ray diffraction (XRD), scanning electron microscopy (SEM) and transmission electron microscopy (TEM). The photocatalytic activity of the CuO NPs was evaluated by degradation of palm oil mill effluent (POME) under UV irradiation, and the extend of POME degradation was observed by measuring chemical oxygen demand (COD) values. The results showed 81 % of the POME was successfully degraded under UV irradiation for 3 hours. The phytotoxicity experiment using mung bean (*Vigna radiata* L.) seed also showed a decreasing in toxicity of POME after photodegradation.

ABSTRAK

SINTESIS DAN PENCIRIAN NANOPARTIKEL KUPRUM(II) OKSIDA YANG DIPEROLEH DARIPADA EKSTRAK KULIT LEMON (*Citrus limon*) UNTUK DEGRADASI FOTOKATALITIK EFLUEN KILANG KELAPA SAWIT

Tan Lee Xian

Pencirian pada skala nonometer adalah jauh berbeza daripada sifat pukal makroscopik mereka. Nanopartikel logam telah digunakan untuk pelbagai aplikasi seperti biosensor, penghantaran ubat terkawal, agen anti-mikrob dalam dan fotomangkin untuk rawatan air sisa. Nanopartikel, disebabkan kecenderungannya untuk merendahkan bahan pencemar di bawah cahaya ultraungu, adalah salah satu kaedah yang sesuai untuk rawatan air sisa. Pada masa kini, terdapat pelbagai kaedah fizikal dan kimia telah digunakan untuk mensintesis nanopartikel. Walau bagaimanapun, terdapat banyak ancaman serius terhadap alam sekitar dengan menggunakan kaedah ini disebabkan oleh penggunaan bahan kimia dan pelarut toksik, penggunaan tenaga yang tinggi, kos yang tinggi dan prosedur yang membosankan. Oleh itu, perlunya untuk "sintesis

hijau" nanopartikel kerana kesederhanaan, tidak toksik, tidak mahal, kecekapan tenaga dan mesra alam. Dalam kajian ini, nanopartikel kuprum (II) oksida, CuO NPs telah disintesis dengan menggunakan ekstrak kulit lemon (LPE) sebagai agen penurunan dan penstabil, dan garam kuprum(II) nitrat trihidrat sebagai prekursor. Ekstrak kulit lemon disediakan dengan air ternyahion dengan pemanasan 20 minit dan penapisan dua kali, dan kuprum(II) nitrat trihidrat ditambah ke dalam LPE dengan pendidihan berterusan dan kacau sehingga pes hijau gelap diperolehi. Kemudian, pes hijau gelap akan dikalsinasi dalam relau pada suhu 450 ℃ selama 2 jam. CuO NPs yang disintesis hijau dicirikan dengan menggunakan spektroskopi UV-Vis, FTIR, EDX, XRD, SEM dan TEM. Aktiviti fotokatalitik CuO NP yang disintesis hijau telah dinilai dengan degradasi efluen kilang kelapa sawit (POME) di bawah penyinaran ultraungu (UV), dan lanjutan degradasi POME diperhatikan dengan mengukur nilai permintaan oksigen kimia (COD). Keputusan menunjukkan 81% POME telah berjaya didegradasi di bawah penyinaran UV dalam masa 3 jam. Eksperimen fitotoksisiti menggunakan biji kacang hijau (*Vigna radiata* L.) juga menunjukkan penurunan ketoksikan POME selepas fotodegradasi.

ACKNOWLEDGEMENTS

First of all, I would like to express my deepest gratitude to my final year project supervisor, Dr. Mohammod Aminuzzaman for his valuable guidance and advices throughout this research. Besides, a special word of thanks also goes to my FYP supervisor for providing the learning opportunities and I had learnt a lot of skill and knowledge.

Furthermore, I would like to deliver my sincere appreciation to UTAR for giving me an opportunity to complete my final year project with the facilities and equipment provided.

Moreover, I want to take this opportunity to thank the lab officers (Mr. Ooh Keng Fei, Mr. Goh Wee Sheng, Mr. Leong Thung Lim, Mr. Seou Chi Kien and Ms. Wong Wei Seng) for suppling the glassware, guiding me in handling the instrument, and providing the help whenever I encounter the problems.

Last but not least, I am feeling grateful to have all my parents, family, and friends for their continuous love, support and encouragement throughout the project.

DECLARATION

I hereby declare that the project report is based on my original work except for quotations and citations which have been duly acknowledged. I also declare that it has not been previously or concurrently submitted for any other degree at UTAR or other institutions.

TAN LEE XIAN

APPROVAL SHEET

This final year project report entitled **"GREEN SYNTHESIS AND CHARACTERIZATION OF COPPER(II) OXIDE NANOPARTICLES DERIVED FROM LEMON (*Citrus limon*) PEEL EXTRACT FOR THE PHOTOCATALYTIC DEGRADATION OF PALM OIL MILL EFFLUENT (POME)"** was prepared by TAN LEE XIAN and submitted as partial fulfilment of the requirements for the degree of Bachelor of Science (Hons) Chemistry at Universiti Tunku Abdul Rahman.

Approved by:

Date: 1st June 2022

(Asst. Prof. Dr Mohammod Aminuzzaman)

Supervisor

Department of Chemical Science

Faculty of Science

Universiti Tunku Abdul Rahman

FACULTY OF SCIENCE

UNIVERSITI TUNKU ABDUL RAHMAN

Date: 1st June 2022

PERMISSION SHEET

It is hereby certified that **TAN LEE XIAN** (ID No: **18ADB02223**) has completed this final year project report entitled **"**GREEN SYNTHESIS AND CHARACTERIZATION OF COPPER(II) OXIDE NANOPARTICLES DERIVED FROM LEMON (*Citrus limon*) PEEL EXTRACT FOR THE PHOTOCATALYTIC DEGRADATION OF PALM OIL MILL EFFLUENT (POME)**"** under supervision of ASST. PROF. DR MOHAMMOD AMINUZZAMAN from the Department of Chemical Science, Faculty of Science.

I hereby give permission to the University to upload the softcopy of my final year project report in pdf format into the UTAR Institutional Repository, which may be made accessible to the UTAR community and public.

Yours truly

_____

(TAN LEE XIAN)

TABLE OF CONTENTS

LIST OF FIGURES

LIST OF TABLES

LIST OF ABBREVATIONS

Å	Angstrom
A_0	Initial absorbance of POME solution
A_t	Absorbance of POME solution at different time interval, t
AOPs	Advance oxidation processes
BOD	Biochemical oxygen demand
c	Speed of light
C	Carbon
CB	Conduction band
CH_4	Methane
cm^{-1}	Wavenumber
CO_2	Carbon dioxide
COD	Chemical oxygen demand
COD_0	Initial COD value of the POME before expose to UV irradiation
COD_t	COD value of the POME after photodegradation at different time interval
Cu^0	Copper atom
CuO	Copper(II) oxide
CuO NPs	Copper(II) oxide nanoparticles
Cu_2O	Cuprous oxide
CVD	Chemical vapor deposition
D	Crystalline size in diameter

DI	Deionized
DO	Dissolved oxygen
DOE	Department of Environment
e^-	Electron
EDX	Energy dispersive X-ray
E_g	Optical band gap energy
EQA	Environmental Quality Act
eV	Electron volt
FESEM	Field emission scanning electron microscopy
FTIR	Fourier transform infrared
FWHM	Full-width half maximum
g	Gram
h	Plank's constant
h^+	Hole
H^+	Hydrogen Ion
HNO_3	Nitric acid
H_2O	Water
H_2O_2	Hydrogen peroxide
ICDD	International centre for diffraction data
JCPDS	Joint committee on power diffraction standards
k	Scherrer constant
K	Potassium
kV	Kilovolt
L_c	Radicle length of control
L_s	Radicle length of samples

LPE	Lemon peel extract
mA	Milliampere
mg	Milligram
mL	Milliliter
mM	Millimolar
M	Molarity
n	Exponent to determine the type of electronic transition
nm	Nanometer
NPs	Nanoparticles
O	Oxygen
O_2	Oxygen molecule
O_2^-	Superoxide anion
OH•	Hydroxyl radical
OH^-	Hydroxide ion
pH	Potential of hydrogen
POME	Palm oil mill effluent
ppm	Part per million
Rpm	Revolution per minute
s^{-1}	Unit of frequency
SEM	Scanning electron microscopy
SPR	Surface plasmon resonance
TEM	Transmission electron microscopy
TiO_2	Titanium dioxide
UV	Ultraviolet
UV-Vis	Ultraviolet-visible

VB	Valence band
XRD	X-ray diffraction
ZnO	Zinc oxide
℃	Degree celsius
α	Absorption coefficient
β	Full width half maximum width (FWHM) of diffraction peak in radian 2θ
θ	Bragg's diffraction angle
ν	Frequency of photon
λ	Wavelength
λ_{max}	Maximum wavelength

CHAPTER 1

INTRODUCTION

1.1 Background of study

'Nano' acquired from Greek, meaning very little. Nanometer is represented one billionth of a meter. Nanoscience studied the structures and molecules from 1 to 100 nanometers (Mansoori and Soelaiman, 2005). American physicist and famous Nobel Laureate, Richard Feynman gave a speech entitled "There's Plenty of Room at the Bottom" by introducing the concept of control matter at the atomic level. In 1974, Japanese physicist named Norio Taniguchi, the first utilized the term "nanotechnology" to describe semiconductor operations on nanoscale. In the year 1985, Fullerenes were discovered by Kroto, Smalley, and Curl. K. Eric Drexler published a book "Engines of Creation: The Coming Era of Nanotechnology." by incorporating ideas from Feynman's "There is Plenty of Room at the Bottom". The term "molecular nanotechnology" is widely used to describe Drexler's view of nanotechnology. Iijima, a Japanese scientist, produced carbon nanotubes in 1991 (Hulla et al., 2015). Throughout the year, nanotechnology has been applied in different fields such as medicine, agriculture, chemistry, and electronics (Bayda et al., 2020).

1.2 Palm oil mill effluent (POME)

Palm oil is extensively consumed as vegetable oil worldwide. Indonesia and Malaysia have led global palm oil output, followed by Colombia, Thailand, and Nigeria. Over 93% of world's palm oil is produced in these countries. 0.72–0.75 tonnes of POME is produced from every tonnes of fresh fruit bunch processing (Izah, 2016). The acidic (pH 4.5-5) POME consists of water (95-96 %), total solids (4-5 %), oil and grease (0.6-0.7 %) (Dashti et al., 2020). Organic materials such as pectin (3400 ppm), phenolics (5800 ppm), lignin (4700 ppm) and amino acids are present in POME. As a result of its high chemical oxygen demand (COD) (40,000-100,000 ppm) and biochemical oxygen demand (BOD) (25000-65000 ppm), POME can have a severe negative impact on the environment if discharged directly into water sources (Phang et al., 2021). When POME released into water bodies, it resulted in anoxygenation and may kill the aquatic organisms, preventing humans from getting the clean water (Iwuagwu and Ugwuanyi, 2014). To protect the aquatic environment, the POME must be treated in accordance with the permissible discharge limit stated by the Department of Environment (DOE) Malaysia and Environmental Quality Act (EQA) 1974.

1.2.1 POME treatment methods

1.2.1.1 Anaerobic ponding system

About 85% of Malaysia's palm oil mills used the anaerobic ponding system for treating the POME because of its cost-effectiveness, system reliability, energy efficiency, and simple design. Organic matters were broken down by various anaerobic microorganisms into methane and carbon dioxide (Abdurahman et al., 2013). However, this traditional POME treatment procedure requires long processing times and large areas for treatment (Mohammad et al., 2021). In addition, the POME treated by the anaerobic ponding system failed to meet the permissible discharge limit stated by the DOE Malaysia and EQA 1974 (Zainuri et al., 2018).

1.2.1.2 Advance oxidation processes

Advanced oxidation processes (AOP) is the technology for the decomposition of organic matters in wastewater that are based on the in situ creation of powerful oxidants, such as hydroxyl radicals. Photocatalysis, fenton-like reactions, and ozonation are examples of AOP. Photocatalytic oxidation systems have been the focus of research because of their low operating costs, as well as the fact that they are sustainable, renewable, and ecologically beneficial (Charles and Cheng, 2018; Saputera et al., 2021).

1.3 Nanoparticles

Nanoparticles (NPs) are small materials that range in size from 1 to 100 nanometers. NPs are composed of three layers, which are surface layer, shell layer and core. Various small molecules can react with the surface layer. The shell layer is chemically and physically different from the core, while the core is the nanoparticle's central component. Nanoparticles have been divided into a number of categories, including metal nanoparticles, fullerenes, ceramic nanoparticles, and polymeric nanoparticles. Because of their large surface area and nanoscale size, NPs have unique physical and chemical characteristics (Khan et al., 2019).

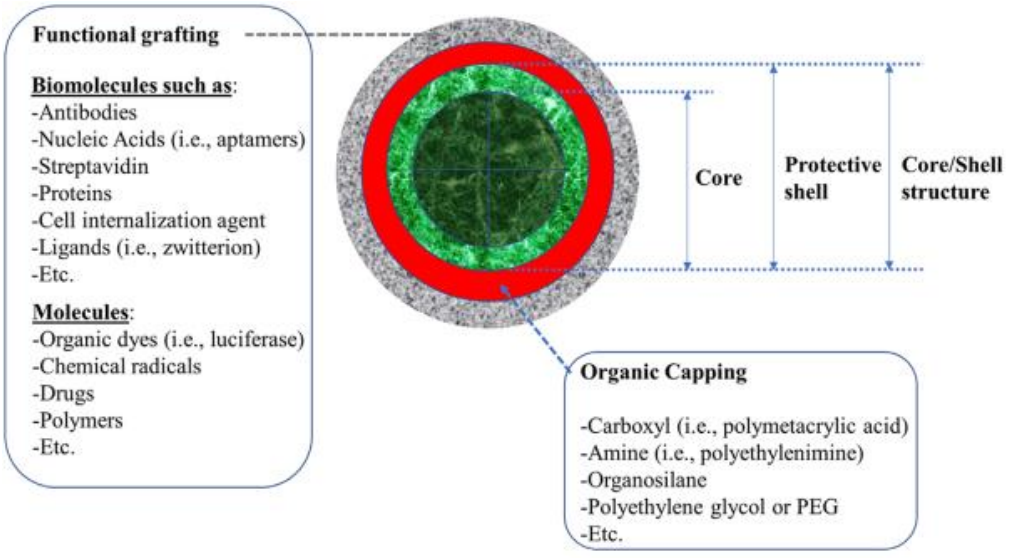

Figure 1.1: Three-layer structure of typical nanoparticles (Feugang, 2017).

1.3.1 Application of nanoparticles

Nanoparticles are unique in that they have great surface area, good optical and chemical properties, making them ideals candidates for a variety of applications. In the current situation where there is a water shortage worldwide, nanoparticles can play a critical role in treating wastewater and making it usable for various processes. Industrial wastewater consists of a variety of heavy metals and organic pollutants, which are harmful to the environment and individual's health. Thus, removal of organic pollutants from wastewater has gained significant attention. Photodegradation of organic pollutants by NPs is a popular practice. The larger surface area NPs are efficient in photodegradation reaction. CuO, TiO_2, and ZnO have the ability in performing photocatalytic degradation of contaminants in wastewaters (Sagir et al., 2020).

In biomedical applications, NPs have the capacity to deliver drugs in the optimal dosage, causing higher therapeutic efficacy, avoiding side effects and enhancing patient compliance. The optical properties of NPs are used in cell imaging and photothermal therapeutic. Moreover, NPs have been applied in mechanical industry, particularly in coatings, lubricants and adhesives. Alumina, titania and carbon based NPs have shown to be successful in achieving the desirable mechanical properties in coatings. In the food industry, some NPs can build an impenetrable barrier to prevent the gases, humidity and other variables that could decrease the food stability. Because of the antibacterial and antioxidant properties of some NPs, the food degradation preventing effect could be

complemented. In cosmetic industry, sunscreen that made from nanometric titanium dioxide and zinc dioxide are paticularly effective at absorbing UV radiation, so they are important in the sunscreens and solar protection products (Martinez et al., 2021). In agricultural field, green synthesized nanoparticles have the potential to improve fertilization process and regulate plant growth (Ghidan and Antary, 2019). For example, iron oxide NPs have been used in biofortification and acted as pesticides.

1.3.2 Synthesis method of nanoparticles

1.3.2.1 Top-down and bottom-up approach

As indicated in Figure 1.2, there are two major methods for synthesizing nanoparticles, which are “top-down” and “bottom-up” methods. The destructive technique is used in the top-down approach. The bigger molecule is breaking down into smaller molecules subsequently converted into nanoparticles. Mechanical milling, sputtering, laser ablation and other decomposition techniques are examples of this method (Figure 1.3). One of the disadvantages of the top-down method is that smaller particles were formed with a broad size distribution. Therefore, the bottom- up approach is more favored as it is simple and precise. The "bottom-up" approach is the building up approach, which forms nanoparticles from assembling atoms and molecules. Chemical vapor deposition (CVD), atomic condensation, laser pyrolysis, and other techniques have been employed (Figure 1.3). CuO NPs that biologically synthesized from bacteria,

fungi and plants are also belongs to bottom-up approach (Ali, 2020). The bottom-up approach produces nanoparticles with less defects and a more homogenous chemical composition.

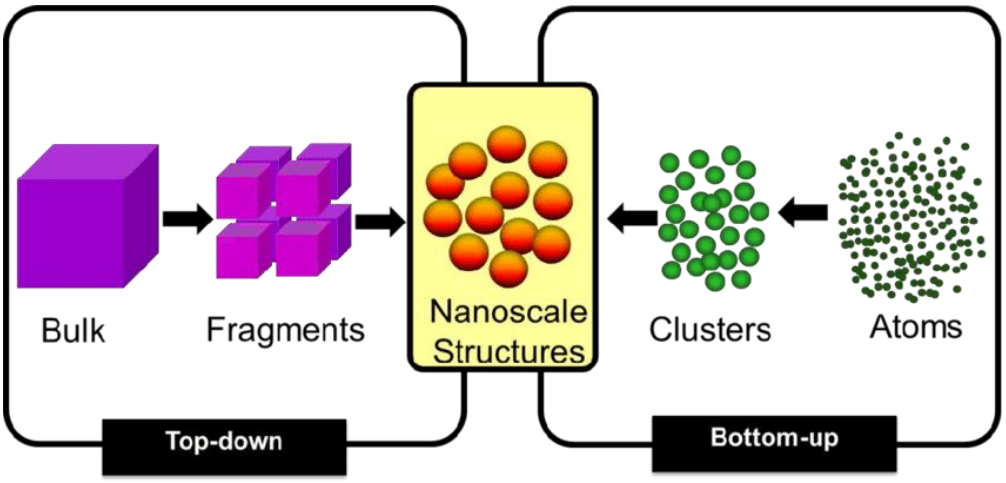

Figure 1.2: Top-down and bottom-up synthesis of nanoparticles (Rawat, 2015).

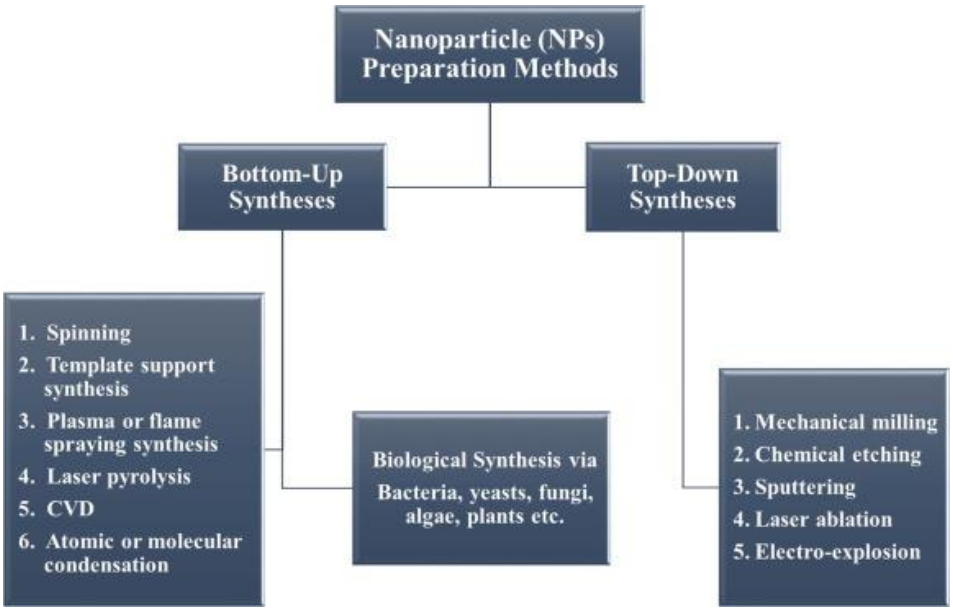

Figure 1.3: Synthesis methods of nanoparticles (Iravani, 2011).

1.3.2.2 Green synthesis of CuO NPs

CuO NPs have been synthesized using various methods, including sol-gel, sonochemical, chemical precipitation, hydrothermal, microwave irradiation, γ-irradiation, electrochemical reduction, solid-state reaction, etc. (Ullah et al., 2017). However, these methods possess a lot of significant problem, such as utilization of noxious chemicals and solvents, consumption of high energy, production of toxic waste, high cost of operation and requiring of tedious procedure (Alhalili, 2022). In comparison, green-synthesized of CuO nanoparticles using plant extracts has gained considerable attention because of its simplicity, nontoxicity, cost effectiveness, energy efficiency, and environmental friendliness (Varadavenkatesan et al., 2021). The plant extracts consist of a number of phytochemicals like alkaloids, flavonoids, amides, aldehydes, polyphenols, proteins, etc., that serve as reducing and stabilizing agent during green synthesis (Singh et al., 2018). Examples of plant materials that can play the role of reducing and stabilizing in the synthesis of CuO NPs are shown in Table 1.1.

Table 1.1: List of CuO NPs synthesized from various plants.

Plant materials	References
Caesalpinia bonducella (seed extract)	(Sukumar et al., 2020)
Carica papaya L. (peel extract)	(Phang et al., 2021)
Cavendish banana (peel extract)	(Aminuzzaman et al., 2017)
Hibiscus Rosa-sinensis (leaves extract)	(Chai et al., 2019)
Madhuca longifolia (flower extract)	(Das et al., 2018)
Opuntia focus-indica (peel extract)	(Badri et al., 2021)
Stachys lavandulifolia (flower extract)	(Veisi et al., 2021)
Tamarindus indica L. (leaves extract)	(Zaman et al., 2020)
Tinospora crispa (leaves extract)	(Apriandanu and Yulizar, 2019)
Triticum aestivum (seed extract)	(Buazar et al., 2019)

1.4 Principle of green chemistry

Green chemistry is the application of a set of principles in the design, manufacture, and application of chemical products that lowers or eliminates the use or synthesis of hazardous compounds. There are twelve principles in the principle of green chemistry (Anastas and Warner, 1998). Some of the principles have been fulfilled during the synthesis and application of CuO NPs, including prevent waste, maximise atom economy, less hazardous chemical syntheses, safer chemicals and products, safer solvents and reaction conditions, reduce derivatization and use of catalyst. Firstly, lemon peel waste has been acted as the reducing agent as well as stabilizing agent in the synthesis of CuO NPs. Owing to its high nutritive and medicinal value, lemon is consumed in large amount

worldwide, causing the generation of huge amount of peel and seed wastes, and this could result in significant problem if the wastes are not dispose properly. Hence, by using the lemon peel for CuO NPs synthesizing, the waste can be prevented. Besides, the synthesizing reaction has high atom economy as high yield of CuO NPs have been obtained. Moreover, water is functioned as the nontoxic, cost effective and renewable reaction medium. In addition, the synthesized CuO NPs have been acted as the photocatalyst in the degradation of palm oil mill effluent (POME), which fulfilled the principle of green chemistry.

Figure 1.4: Twelve principles of green chemistry (Harrison et al., 2021).

1.5 Copper (II) oxide nanoparticles (CuO)

Semiconductor nanostructured-based materials have gained significant attention as photocatalysis in the degradation of various organic pollutants like dyes, surfactant, pesticides, phenolic compounds, etc. into harmless products under light irradiation. CuO NP is a semiconductor type-*p* with 1.2 eV of band gap. Owing to its superior characteristics, such as excellent optical, electrical, magnetic, catalytic, and biological properties, CuO nanoparticles have been utilized in various applications, including catalysis, solar cell, magnetic storage media, lithium battery, biosensor, gas sensor, antimicrobial agents in the agriculture and health sectors, and photocatalysts for wastewater treatment, etc. (Grigore et al., 2016).

1.6 Photocatalytic activity of CuO NPs

CuO NP is a semiconductor that can generate electron-hole pairs (e/h^+) as a result of the excited electrons in the valance band transited to the conduction band and forming holes in the valence band after absorbing photon energy ($h\nu$) from UV light (Equation (1)). If there are compounds adsorbed on the surface of the semiconductor, the redox process begins. To avoid recombination, a good scavenger will take this electron–hole pair (Equation (2)). Superoxide radicals (O_2•) are formed when electrons in the conduction band combine with oxygen (Equation (3)), while holes in the valence band react with water molecules (H_2O) to form hydroxyl radicals (OH•) (Equation (4)). Hydroperoxyl radical

production (Equation (5)) converts superoxide radicals to hydrogen peroxide (Equation (6)). In the presence of light, hydrogen peroxide is transformed to hydroxyl radical (Equation (7)). Pollutants are degraded by these radicals (hydroxyl radical, superoxide radical, and hydrogen peroxide) into tiny harmless molecules like CO_2, H_2O, and mineral acids (Equation (8)). The photocatalytic degradation mechanism of pollutant using CuO NPs is shown in Figure 1.5.

$$\text{CuO NPs} + h\nu \text{ (UV light)} \rightarrow e_{CB}^{-} + h_{VB}^{+} \quad (1)$$

$$\text{CuO NPs } (e_{CB}^{-} + h_{VB}^{+}) \rightarrow \text{CuO NPs} + \text{heat} \quad (2)$$

$$e_{CB}^{-} + O_2 \rightarrow O_2\bullet^{-} \quad (3)$$

$$h_{VB} + + H_2O \rightarrow H^{+} + OH\bullet \quad (4)$$

$$O_2\bullet^{-} + H^{+} \rightarrow OOH\bullet \quad (5)$$

$$2\ OOH\bullet \rightarrow H_2O_2 + O_2 \quad (6)$$

$$H_2O_2 + h\nu \rightarrow 2\ OH\bullet \quad (7)$$

$$\text{pollutant} + (OH\bullet, O_2\bullet^{-}) \rightarrow H_2O + CO_2 \quad (8)$$

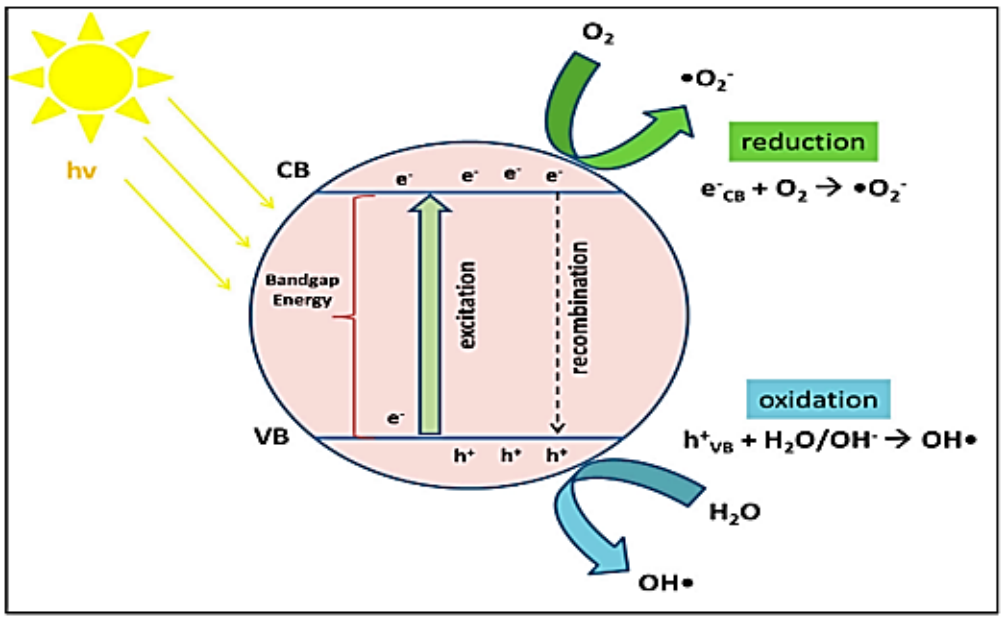

Figure 1.5: Photocatalytic degradation mechanism of pollutant using CuO NPs (Saputera et al., 2021).

1.7 Lemon (*Citrus limon*)

Citrus limon (Figure 1.6) is a tiny evergreen tree species from Rutaceae family (Dev and Nidhi, 2016). Lemon fruit is rich in nutrients, making it an important part of a healthy diet. *Citrus limon*'s therapeutic activities include anti-inflammatory, antibacterial and anticancer. *Citrus limon* juice is commonly used to treat sore throats, fevers, rheumatism and high blood pressure (Klimek-Szczykutowicz et al., 2020). Lemon contains various interesting source, such as flavonoids, minerals, vitamins, essential oils, organic acids, and carotenoids (Mamade et al., 2020). These phytoconstituents play the vital role to reduce and stabilize the CuO NPs during the synthesis.

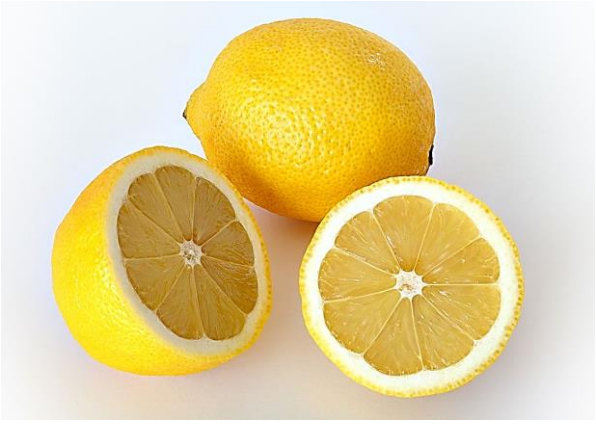

Figure 1.6: *Citrus limon*.

1.8 Objectives of study

1. To synthesize copper(II) oxide nanoparticles (CuO NPs) using lemon (*Citrus limon*) peel extract as reducing as well as stabilizing agent.

2. To characterize the CuO NPs using various analytical tools such as UV-visible spectroscopy (UV-vis), fourier transform infrared spectroscopy (FTIR), X-ray diffraction (XRD), energy dispersive X-ray spectroscopy (EDX), scanning electron microscopy (SEM) and transmission electron microscopy (TEM).

3. To evaluate the photocatalytic performance of green synthesized CuO NPs in the degradation of palm oil mill effluent (POME) under UV irradiation.

4. To determine the possible usage of treated POME for irrigation purpose and its environmental impact by conducting the phytotoxicity test using mung bean (*Vigna radiata* L.) seed.

CHAPTER 2

LITERATURE REVIEWS

2.1 Green synthesis of CuO NPs

Nowadays, many researchers are focused on green chemistry routes in synthesizing environmentally friendly copper (II) oxide nanoparticles that avoiding the use of expensive and noxious chemicals. The CuO nanoparticles synthesized from plant extracts and microorganisms have gained a lot of attention to the scientists and researchers. However, the synthesis of CuO NPs using plant extracts were more favorable because it is easy to carry out, cost-effective, and compatible with the biomedical applications (Amin et al., 2021).

2.1.1 Green synthesis of CuO NPs using plant extracts

Zaman et al. (2020) reported the green and biosynthesis of CuO NPs using *Tamarindus indica* L. leaf extract. *Tamarindus indica* L. is a leguminous tree with edible fruit that belongs to the family Fabaceae. In this study, 15 mL of leaf extract was mixed with 150 mL of 0.1 M of copper (II) chloride dehydrate solution with continuous stirring for 12 hours to obtain the black powder CuO.

Figure 2.1: *Tamarindus indica* L. (Komakech et al., 2019).

Green-synthesized of CuO NPs were characterized by FT-IR, XRD, EDX, SEM and TEM analysis. FT-IR measurement was carried out to detect the phytochemicals presented in the extract which functioned as the reducing and capping agent. A broad band at 3392 cm^{-1} was due to the OH group of citric acid, malic acid and tartaric acid present in the extract. A peak at around 1730 cm^{-1} ascribed to the carbonyl stretching vibrations of the acid groups. A sharp peak at 1625 cm^{-1} and 1395 cm^{-1} represented the H-O-H bending and O-C-O stretching of the esters respectively. An absorption peak at 1084 cm^{-1} was due to the C=O and C-H groups of citric acid. Peaks in between 800–650 cm^{-1} corresponded to the C-H bending of aromatic phenols. A sharp absorption peak at 600 cm^{-1} confirmed the formation the CuO NPs. Based on XRD result, the observed diffraction peaks proved the formation of CuO NPs with monoclinic phase and crystalline nature. The average crystalline size of CuO NPs calculated by using Debye-Scherrer equation and was 23 nm. In EDX analysis, the copper and oxygen element were presented with percentage of 52.9 % and 47.1 % respectively. Based on the SEM image, the CuO NPs were shown in spherical shape, while the size of CuO NPs were observed 50-100 nm in TEM image. In

this study, the green-synthesized CuO NPs degraded Rhodamine B dye successfully about 65% in 2 hours under UV light irradiation.

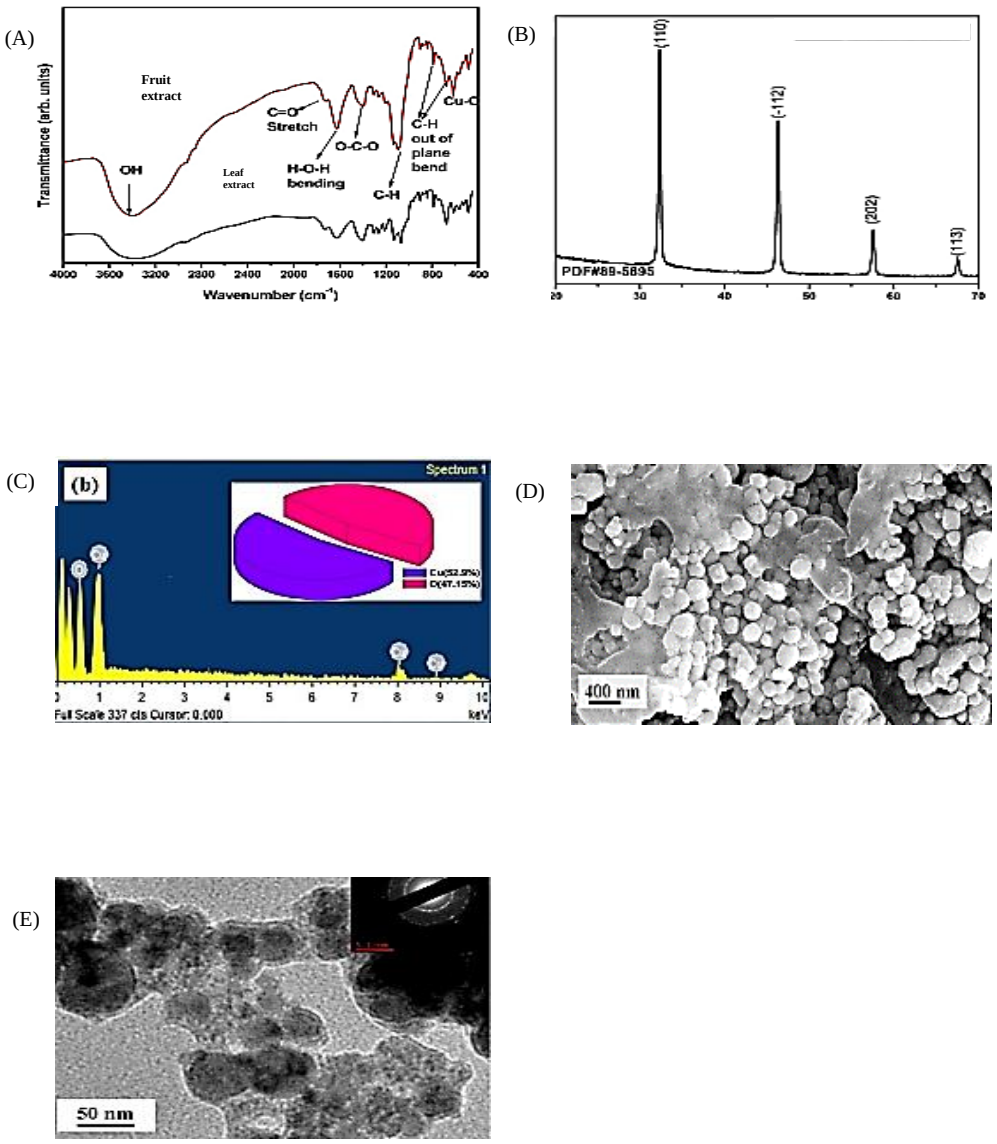

Figure 2.2: (A) FT-IR (B) XRD (C) EDX (D) SEM and (E) TEM image of CuO NPs (Zaman et al., 2020).

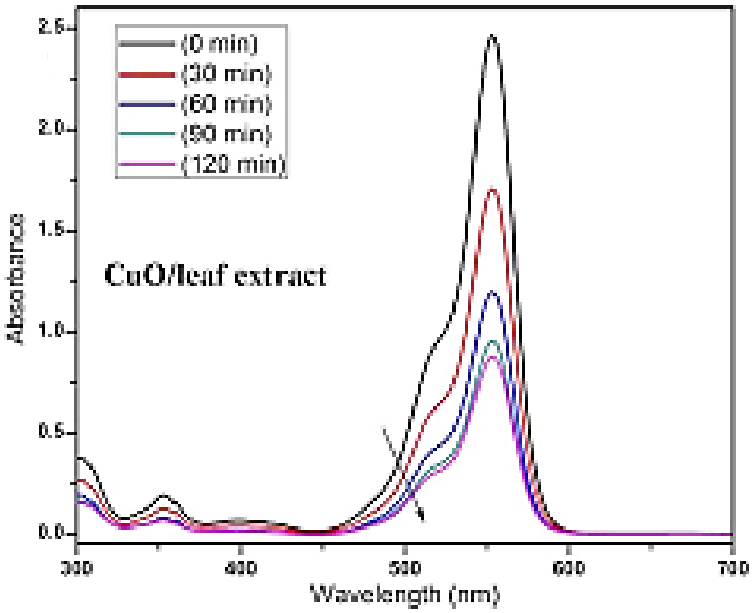

Figure 2.3: Photocatalytic activity of CuO NPs (Zaman, et al., 2020).

Veisi et al. (2021) described the biosynthesis of CuO NPs using *Stachys lavandulifolia* flower extract. *Stachys lavandulifolia* is a flowering plant in the Lamiaceae family. In this study, 100 mL of 1 mM copper (II) acetate solution was added into 10 mL of flower extract of *Stachys lavandulifolia* with heating at 80 °C for 100 min. The sediment formed was dried 48 h in air.

Figure 2.4: *Stachys lavandulifolia* (Sharma et al., 2013).

Biosynthesized CuO NPs were characterized by UV-Vis, FT-IR, XRD, SEM, EDX and TEM. The peak at 400 nm in UV-vis spectrum and 592 cm^{-1} in FT-IR spectrum indicated the successful formation of CuO NPs. Peak at 3400 cm^{-1} was due to free hydroxyl groups. Peak occurred at 1627 cm^{-1} was due to the carbonyl stretching. The bands occurred at 1263, 1174 and 1051 cm^{-1} were assigned to amides, ethers and aliphatic groups that act as capping agent. The XRD diffraction peaks matched well with JCPDS standard no. 01-080-0076, revealing the monocyclic crystalline nature of CuO NPs. SEM image revealed the CuO NPs were in spherical shape with size range of 20-35 nm. EDX spectrum showed the presence of C, N, Cu and O in the synthesized CuO NPs. Carbon and nitrogen atoms were due to the phytoconstituents from the plant extract. CuO NPs with particle size of 15-25 nm without agglomeration were shown in TEM image.

(a)

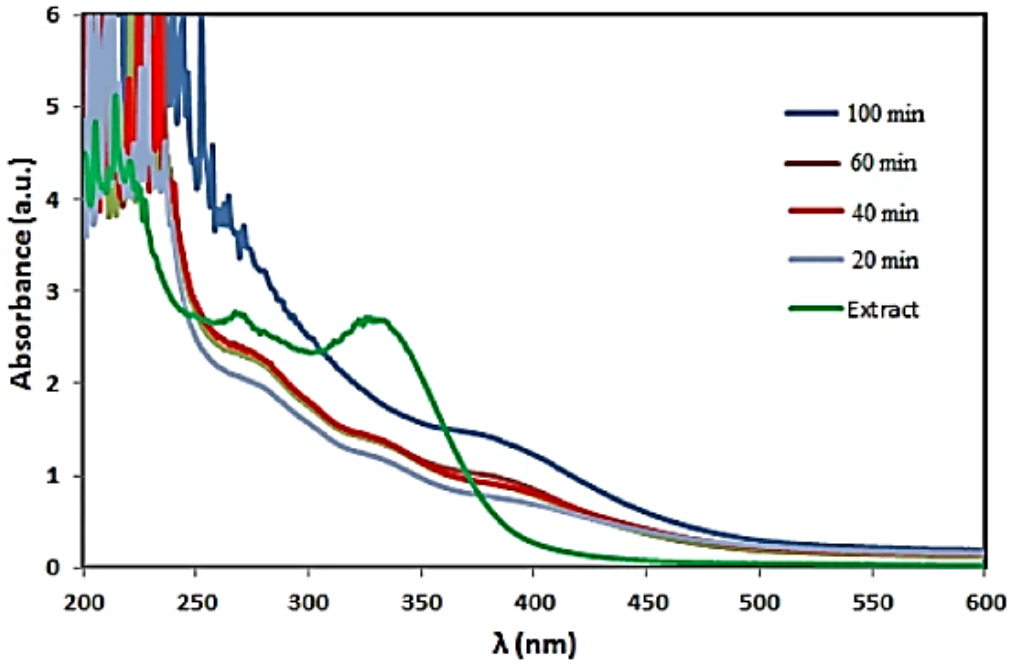

(b)

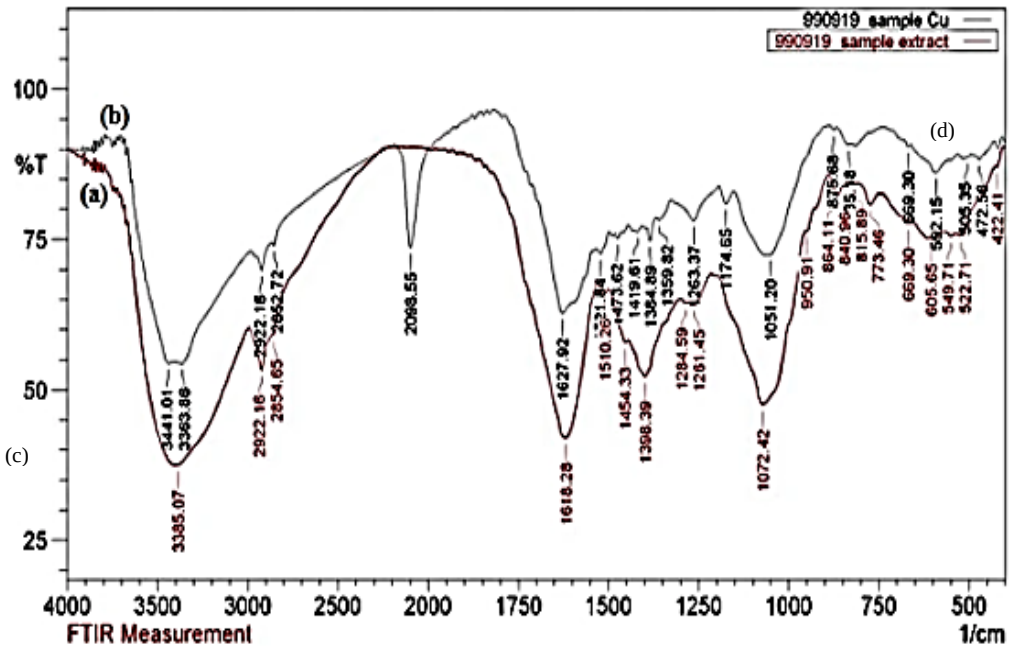

Figure 2.5: (a) UV-vis and (b) FT-IR spectrum of biosynthesized CuO NPs (Veisi et al., 2013).

(c)

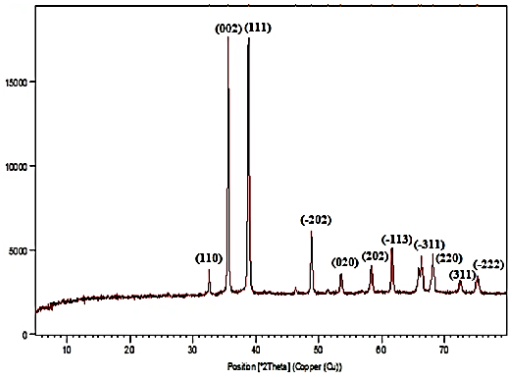

(d)

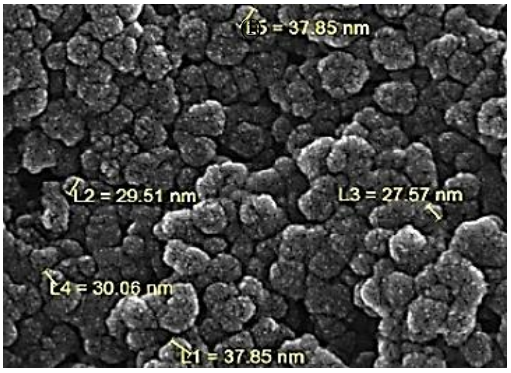

(e)

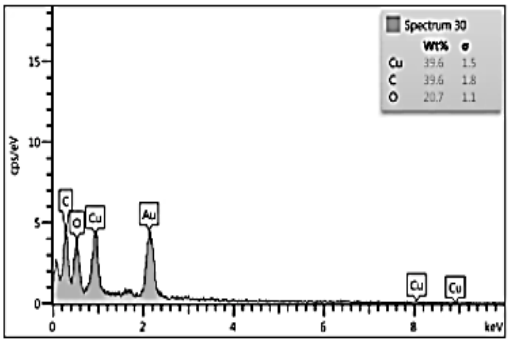

(f)

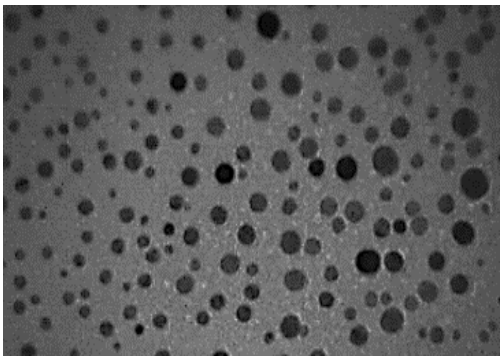

Figure 2.6: (c) XRD (d) SEM (e) EDX and (f) TEM image of biosynthesized CuO NPs (Veisi et al., 2013).

Buazar et al. (2019) reported the synthesis of CuO using *Triticum aestivum* seed extract. Firstly, the wheat grains were dried for 2 days at temperature of 60 ℃, which then grounded into powder. 5 g of *Triticum aestivum* powder was added to 300 mL of DI water to make aqueous extract. After that, 10 mL of *Triticum aestivum* extract was mixed with 90 mL of 0.01 M copper (II) sulfate solution and stirred continuously for 1 hour. It was then subjected to calcination at 95 ℃ for 120 min to obtain CuO NPs.

Figure 2.7: *Triticum aestivum* (Burkart et al., 2015).

UV-vis, FTIR, XRD, SEM and TEM were used to characterize the CuO NPs. In UV–vis analysis, broad absorption peak at 305 nm represents the surface plasmon resonance of CuO NPs. The band gap energy of CuO NPs that obtained using Tauc plot was 4.13 eV. In FT-IR analysis, an intense peak at 483 cm^{-1} represented the Cu-O bond. Absorption peaks observed at 3328 cm^{-1} was assigned to O-H stretching. The CuO NPs' crystallographic nature and phase purity were determined by XRD. From the XRD result, the observed diffraction peaks agreed well with the standard JCPDS01-080-1268, confirming the

formation of monoclinic CuO NPs. CuO NPs have an average crystalline size of 20.76 nm. SEM image showed the spherical shape CuO NPs with size range 21-42 nm. TEM micrograph showed the monodispersed spherical CuO NPs with diameter of 5-40 nm. CuO NPs degraded successfully organic pollutant 4-Nitrophenol by 99.5 % in 20 min under UV irradiation.

(a) (b)

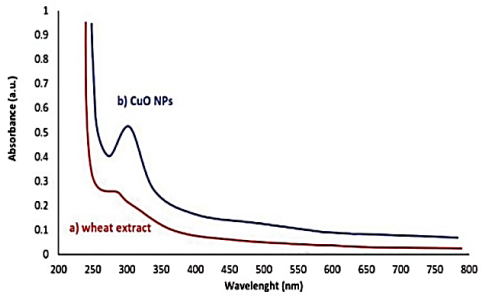

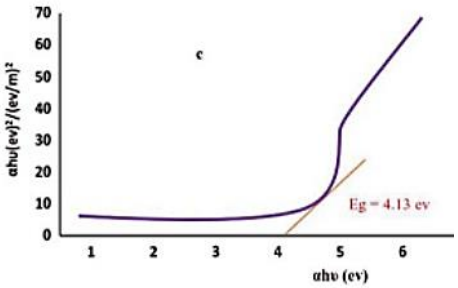

(c) (d)

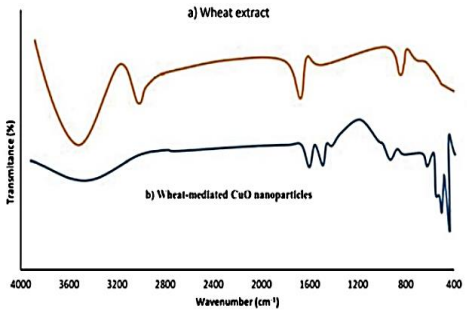

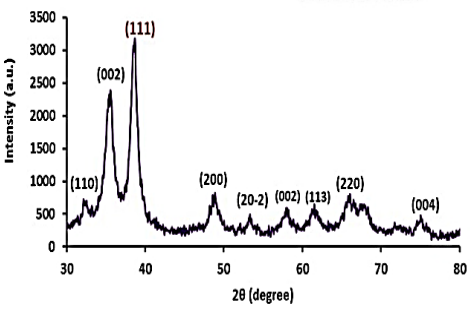

(e) (f)

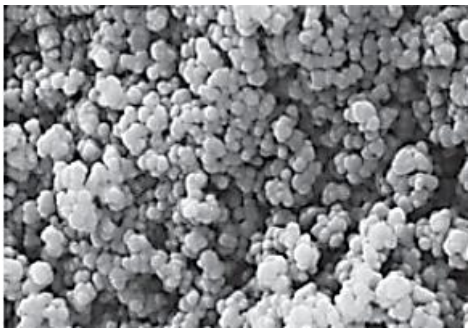

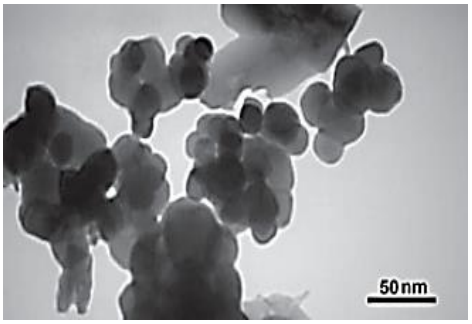

Figure 2.8: (a) UV-vis spectrum (b) Tauc plot (c) FT-IR spectrum (d) XRD spectrum (e) SEM image (f) TEM image of biosynthesized CuO NPs (Buazar et al., 2019).

2.1.2 Green synthesis of CuO NPs using fruit extracts

Phang et al. (2021) described the biosynthesis of CuO NPs using *Carica papaya* L. peel extract. *Carica papaya* contains large amount of *β*-carotene, vitamin (B, C, E), minerals (Na, K, Fe, Ca), and fiber. Papaya juice is consumed because it can treat various diseases such as constipation, diabetes, cancer, heart stroke, etc. *Carica papaya* L. is rich in phytoconstituents like phenolic compounds, flavonoids, catechin, etc. that functioned as capping and reducing agent. The first step in synthesizing of CuO NPs is the addition of 1 g of 0.004 mol of copper (II) nitrate trihydrate to 40 mL papaya peel extract (PPE) and heated at 70-80 ℃ by stirring constantly. After that, the solution was changed from green solution to dark green paste. Lastly, the paste was calcinated at 450 ℃ for 2 hours in order to obtain black powder of CuO NPs.

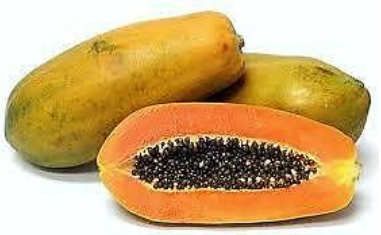

Figure 2.9: *Carica papaya* L. (Saha et al., 2018).

Various analytical tools such as UV-vis, FT-IR, XRD, SEM, EDX and TEM were used to characterize CuO NPs derived from papaya peel. The UV-Vis spectrum of synthesized CuO NPs absorbed at 270 nm, which was due to the resonant oscillating of electrons at the conduction band, that triggered by the

incident electromagnetic radiation. The CuO NPs' band gap energy (E_g) obtained was 3.3 eV using a Tauc's plot. For a better understanding of the formation of CuO NPs, FT-IR spectrum of papaya peel extract (PPE) was compared with that of CuO NPs. In FTIR spectrum, CuO NPs showed a sharp absorption band at 532 cm^{-1}, that was not detected in PPE, revealing the Cu-O bond. The peak at 1412 cm^{-1} for PPE, shifted peak at 1384 cm^{-1} for CuO NPs, and peak at 618 cm^{-1} represented the O-H bending of the phenolic group. Absorption peaks at 1076 cm^{-1} in the spectra of PPE and 1120 cm^{-1} for CuO NPs were due to the C-O stretching. PPE and CuO NPs absorbed at 1636 and 1647 cm^{-1} respectively, showed the presence of primary amide groups. The peaks at 3400 cm^{-1} for PPE and 3368 cm^{-1} for CuO NPs ascribed to the O-H stretching. Finally, phytochemicals in *Carica papaya* such as phenolic compounds, flavonoids, catechin, etc. were played an important role as bioreducing agents in synthesizing CuO NPs. In XRD result, the diffraction peaks of CuO NPs matched well with ICDD: Entry number-00-045-0937, which confirms the synthesized CuO NPs are in monoclinic phase with crystalline structure. The CuO NPs' crystalline size that calculated by Debye-Scherrer equation was 28.06 nm. SEM image revealed the CuO NPs formed were agglomerated spherical in shape with a discrete rough appearance and particle size ranged from 85-140 nm. Only copper and oxygen elements were found in the EDX spectrum, meaning high purity of the CuO NPs had been synthesized. TEM image showed the CuO NPs were agglomerated in lump with a diameter of 277-500 nm. In this study, papaya peel-derived CuO NPs were used as photocatalyst to degrade palm oil mill effluent (POME) under UV-light irridiation. The POME was degraded

successfully with reduction of 66 % COD value in 3 hours using CuO NPs photocatalyst and the POME's phytotoxicity level was reduced to 3.0 %.

(a)

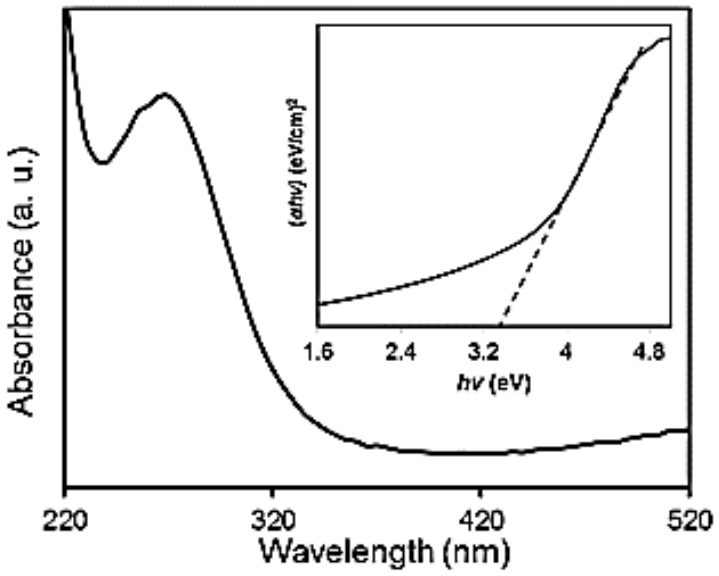

(b)

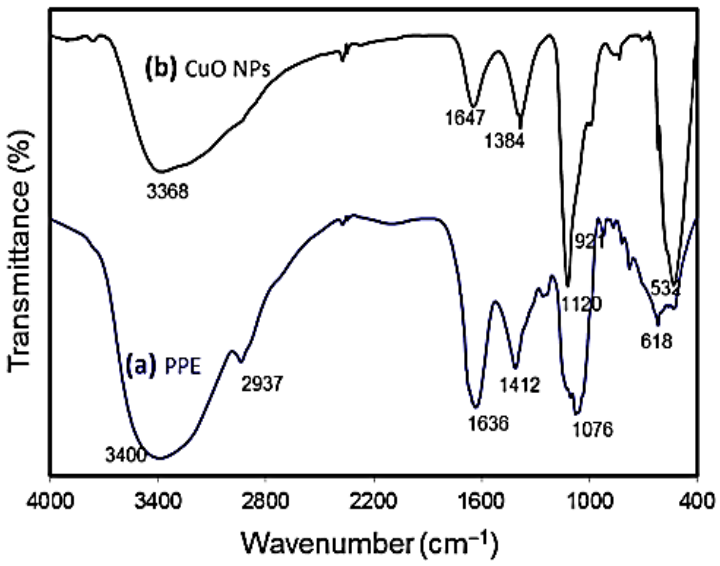

Figure 2.10: (a) UV-Vis and (b) FT-IR spectrum of green synthesized CuO NPs (Phang et al., 2021).

(c)

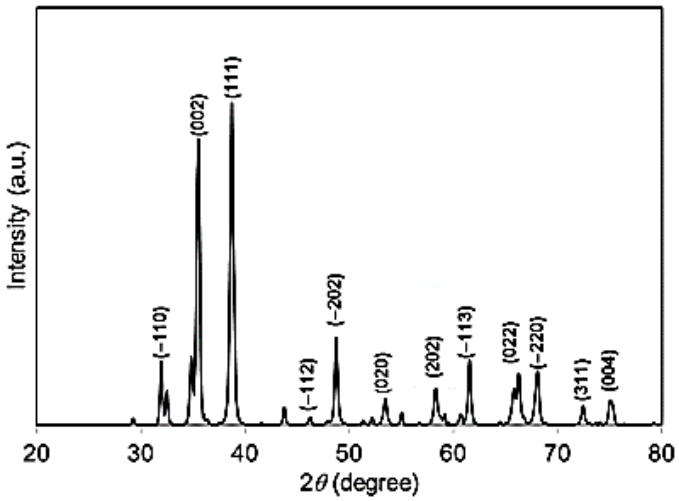

(d)

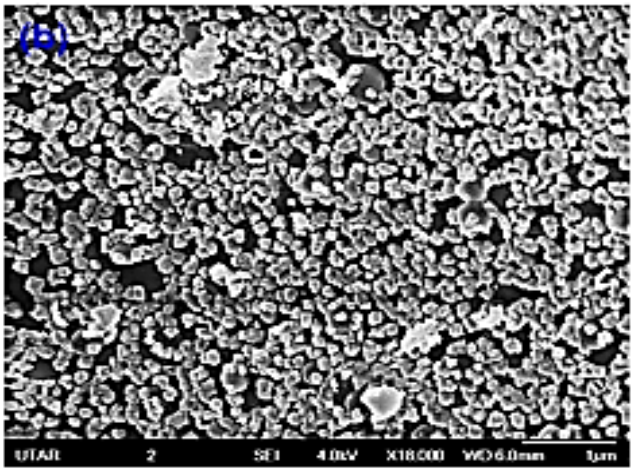

(e)

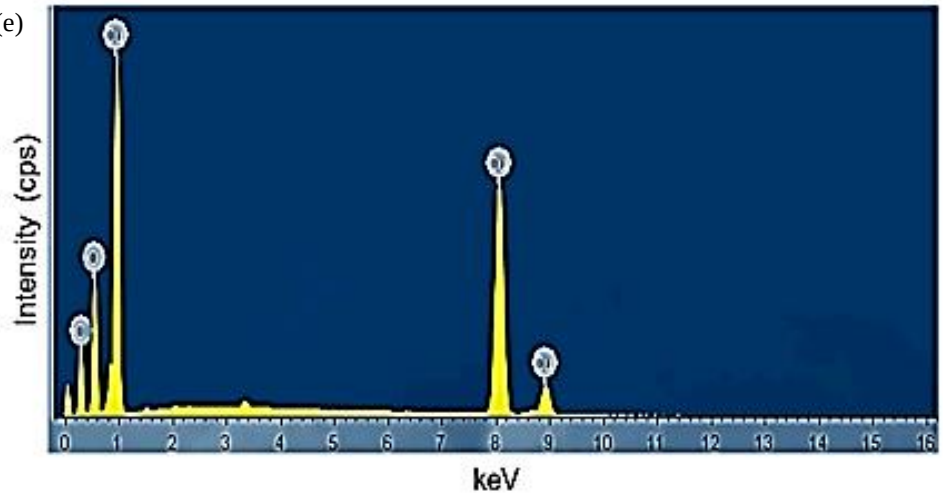

Figure 2.11: (c) XRD (d) SEM and (e) EDX spectrum of green synthesized CuO NPs (Phang et al., 2021).

(f)

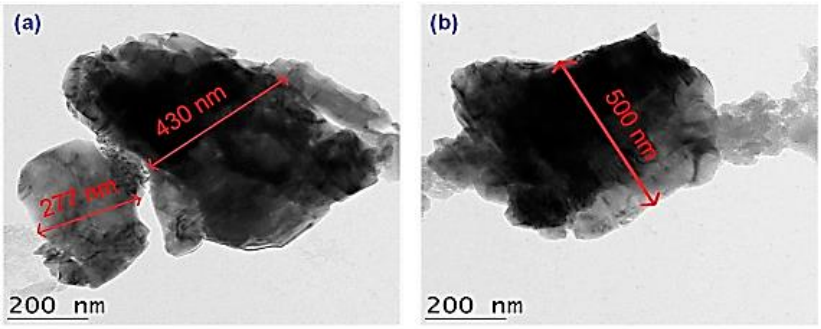

Figure 2.12: (f) TEM image of green synthesized CuO NPs (Phang et al., 2021).

(A)

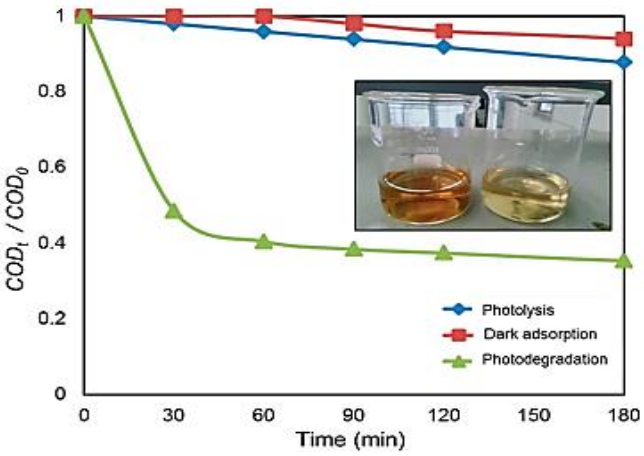

(B)

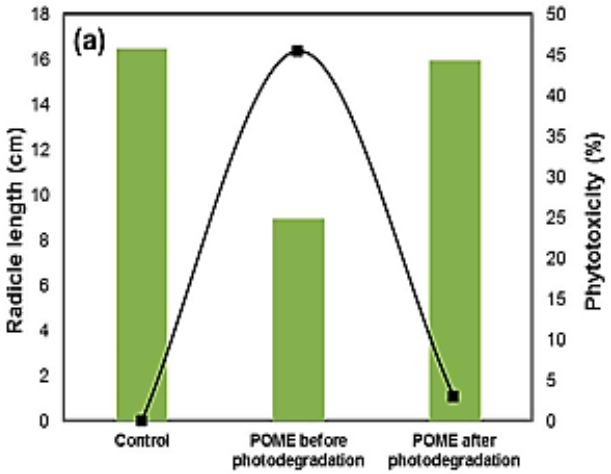

Figure 2.13: (A) Photocatalytic degradation of palm oil mill effluent (POME) by CuO NPs at different condition and (B) Phytotoxicity of POME (Phang et al., 2021).

Ragunath et al. (2021) described the green synthesis of CuO NPs using rambutan peels extract. Rambutan is the tropical tree in the family Sapindaceae. The synthesis process of CuO NPs was performed by adding 10 mL of rambutan peel extract to 50 mL of 0.1 M copper sulfate pentahydrate solution and heating at temperature of 80 ℃ for 2 hours with continuous stirring. Pure copper oxide nanoparticles were obtained after calcination at 450 ℃.

Figure 2.14: Rambutan (Khairy et al., 2015).

The green-synthesized CuO NPs were characterized by UV-Vis, XRD, SEM and TEM. A broad peak located at 370 nm which confirm the Cu-O bond. The diffraction peaks matched with JCPDS data (89-2529) and the crystallite size calculated was 35.74 nm by Debye-Scherrer equation. SEM micrographs showed the synthesized CuO NPs were in flake-like structure with aggregation and had a 20-50 nm size range. TEM image revealed the CuO NPs were agglomerated with average particle size of 40 nm.

(a)

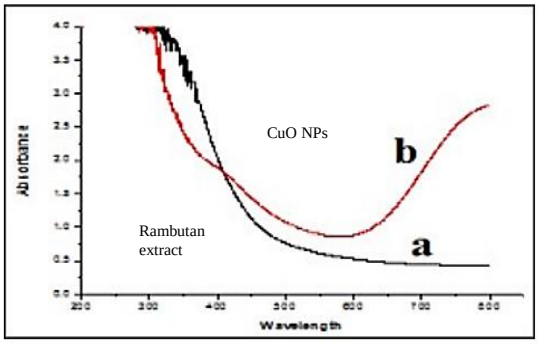

(b)

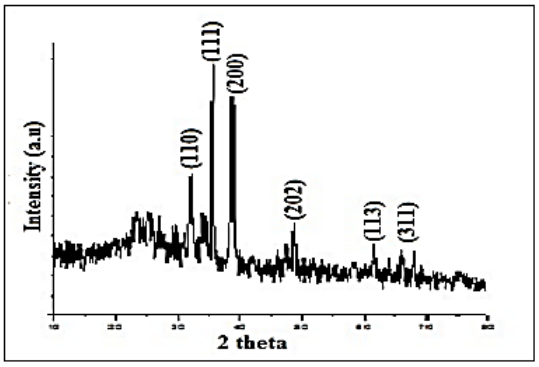

(c)

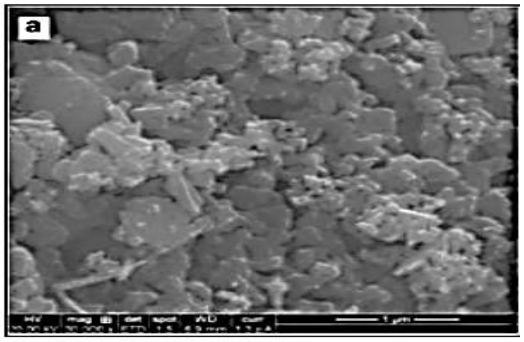

(d)

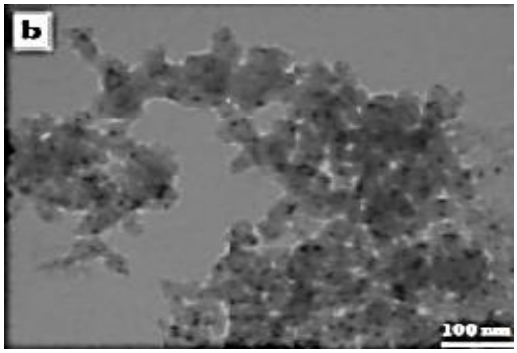

Figure 2.15: (a) UV-vis spectrum (b) XDR spectrum (c) SEM image and (d) TEM image of synthesized CuO NPs (Ragunath et al., 2021).

Badri et al. (2021) reported the green synthesis of CuO NPs using prickly pear (*Opuntia focus-indica*) peel extract. Prickly pear is the fruit of Cactus pear, and belongs to Cactaceae family. In synthesizing process, 0.1 M of copper sulfate pentahydrate solution was mixed with the prickly pear extract with continued stirring until the solution changed into dark brown colour. The nanoparticles were put in the oven for 12 h at 50 ℃ to obtain pure CuO NPs.

Figure 2.16: Prickly pear (*Opuntia focus-indica*) (Dehbi et al., 2013).

The green-synthesized CuO NPs were characterized by UV-Vis, FT-IR, XRD, SEM, EDX and TEM. CuO NPs absorbed at 292 nm, revealing the formation of CuO NPs. Based on the results in FTIR spectrum, a peak occurred at 3285 cm^{-1} and 2926 cm^{-1} were corresponded to the O-H bond of the hydroxyl groups and N-H stretching vibrations of the amine group respectively. The peaks at 1625 cm^{-1} and 1034 cm^{-1} represented the cyclic alkene C=C amine stretching vibrations and carboxylic and phenolic groups respectively. The sharp band at 426 cm^{-1} were the Cu-O bond. Cuprous oxide, Cu_2O bands typically occurred between 605 and 660 cm^{-1} have not detected in the spectrum, meaning high purity CuO NPs was obtained. The diffraction peaks of CuO in XRD result were

well agreed with JCPDS card no. 96-901-4581, confirming the formation of monoclinic phase with crystalline structure CuO NPs. The crystallite size of CuO NPs was found to be in average of 40 nm. The CuO NPs were in spherical shape as shown by SEM image. In EDX spectrum, the percentages for Cu and O were 78.88 % and 21.12 % respectively. No peak other than the copper and oxygen was observed, showing the high purity CuO NPs have been synthesized. The CuO NPs have size distribution ranged from 20 to 60 nm as shown by TEM micrograph.

(a)

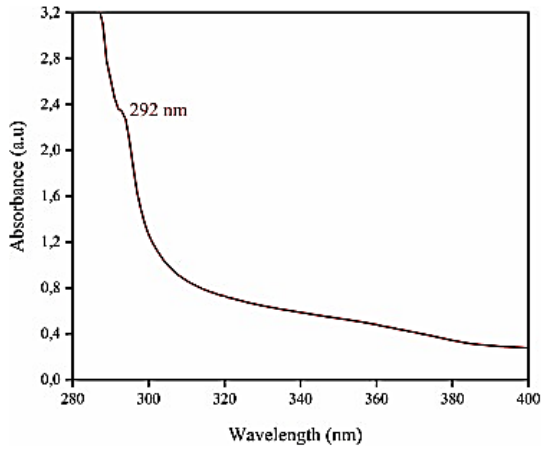

(b)

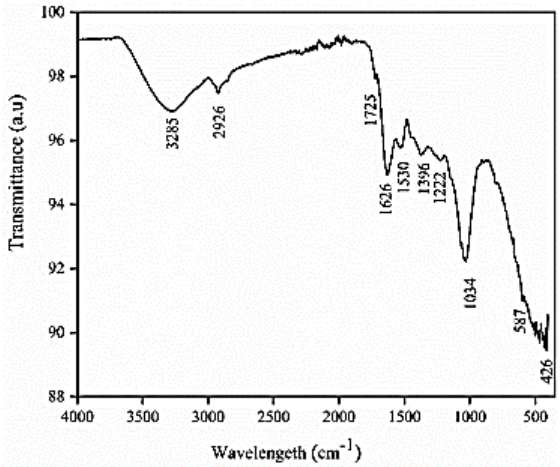

Figure 2.17: (a) UV-Vis spectrum and (b) FT-IR spectrum of green synthesized CuO NPs (Badri et al., 2021).

(c)

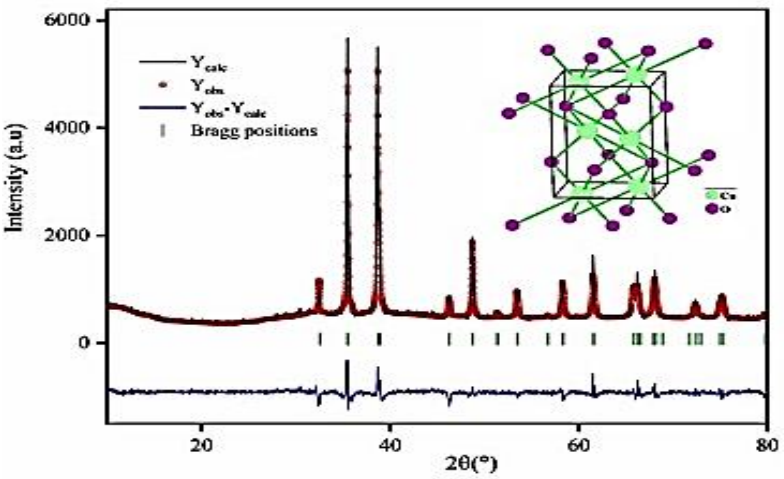

(d)

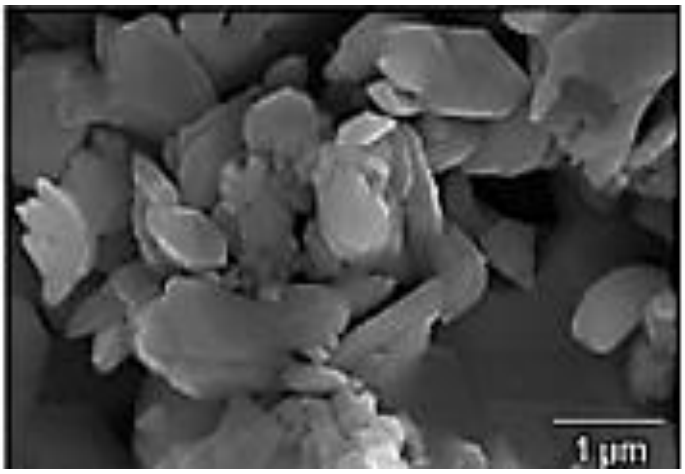

(e)

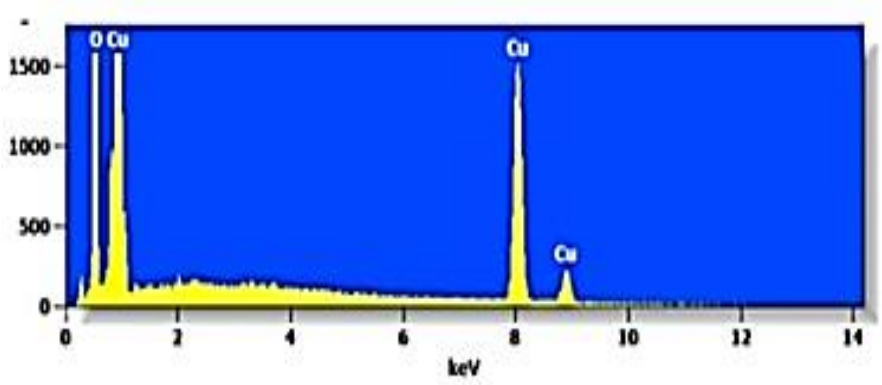

Figure 2.18: (c) XRD spectrum (d) SEM image and (e) EDX spectrum of green synthesized CuO NPs (Badri et al., 2021).

(f)

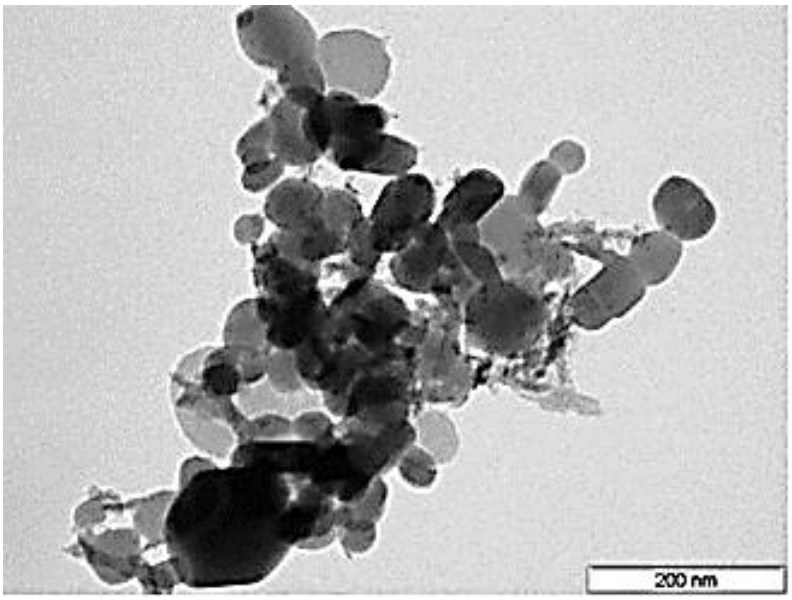

(g)

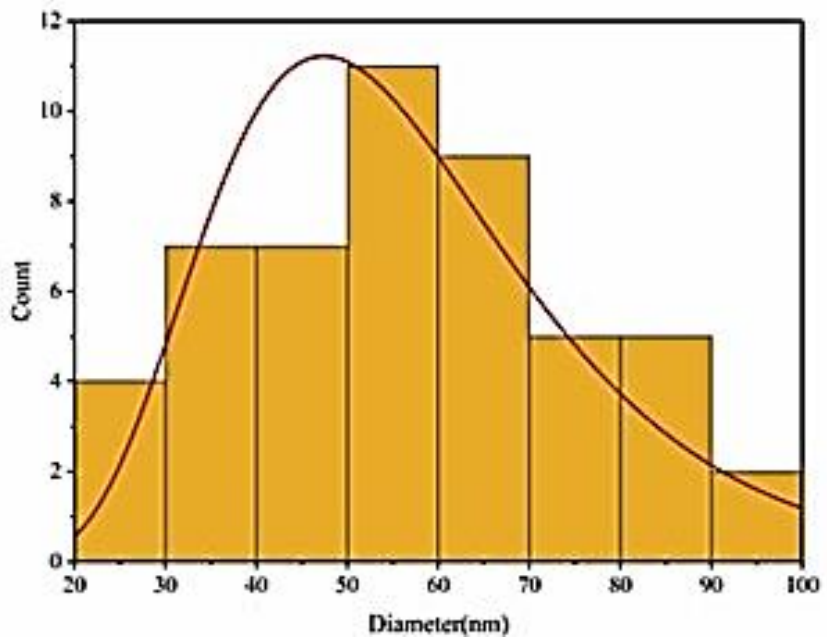

Figure 2.19: (f) TEM image and (g) TEM micrograph of green synthesized CuO NPs (Badri et al., 2021).

2.2 Photocatalytic degradation of POME using nanomaterials

Chai et al. (2019) reported the use of green-synthesized ZnO NPs as photocatalyst to degrade POME under UV-light. Figure 2.20 (a) represented the degradation of POME under different situations. 15% of COD was reduced under dark condition in the presence of ZnO NPs. In photolysis case, the solution without the presence of the ZnO NPs was put under UV light irradiation and 19% of COD has been removed. It showed that POME resist strongly toward the UV irradiation. 82% of COD removal was achieved after 4 hours UV light irradiation in the presence of synthesized ZnO. The POME's phytotoxicity before and after undergoing photodegradation was assessed using mung bean (*Vigna radiata* L.) seed to determine whether the treated POME can be used for irrigation purpose and its environment impact. The radical length of *Vigna radiata* seeds determine the phytotoxicity level. The phytotoxicity of POME before and after the photodegradation was 51.57 % and 6.38 % respectively.

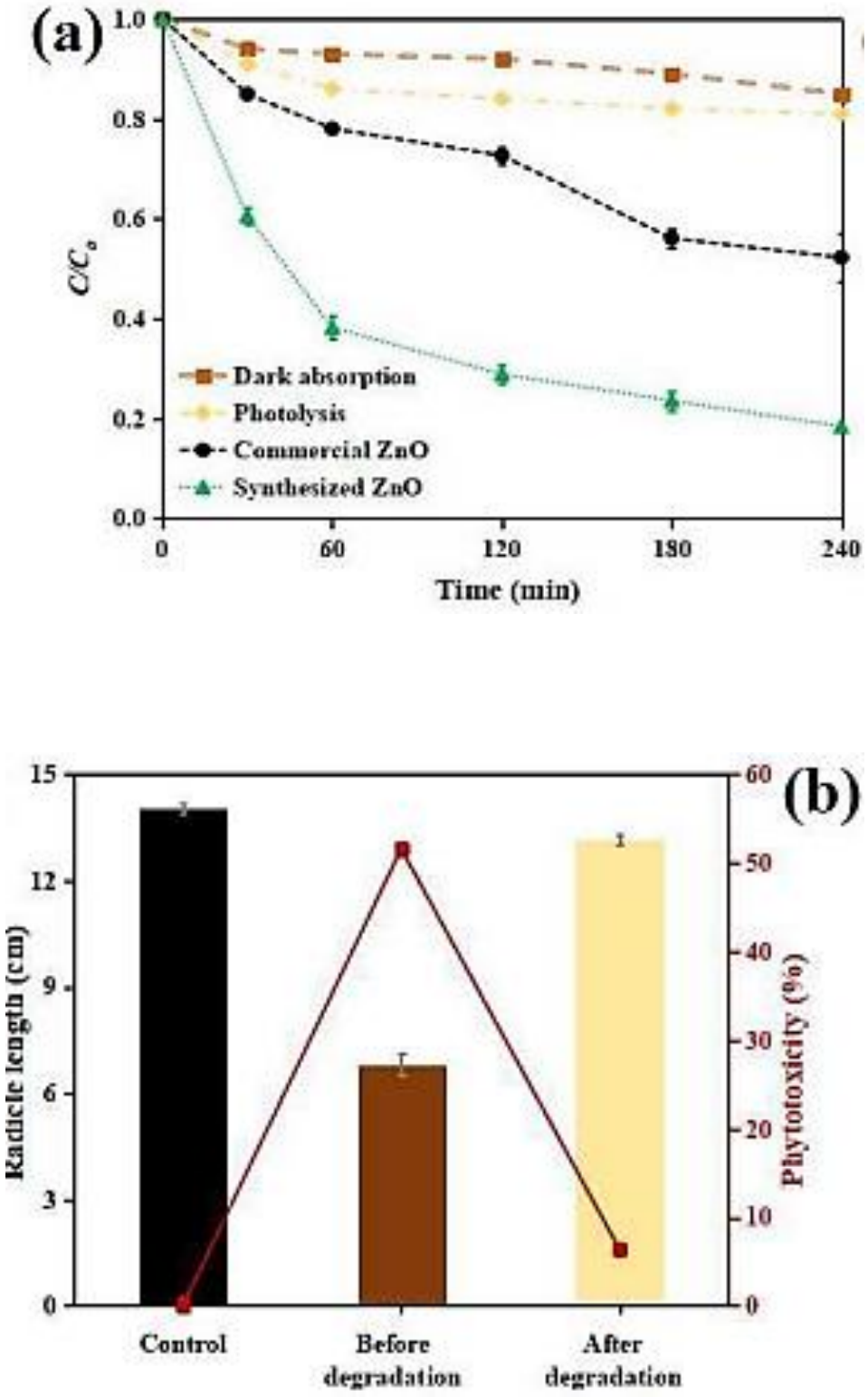

Figure 2.20: (a) Photocatalytic degradation of palm oil mill effluent (POME) at different condition using ZnO NPs and (b) Phytotoxicity of POME before and after photodegradation (Chai et al., 2019).

Cheng et al. (2021) described the degradation of palm oil mill effluent using tungsten trioxide (WO_3) nanoparticles. The degradation of POME was monitored by chemical oxygen demand (COD). Based on Figure 2.21(a), the degradation of POME occurred in the absence of WO_3 NPs was very little, which reveals that photolysis was weak. Besides, the adsorption study that carried out in the absence of WO_3 NPs under dark condition also did not show a reduction in the normalized COD value significantly, indicating that the adsorption of organic substances was minor. WO_3 has inorganic property, so it does not have strong affinity towards the organic substrates, thus only weak adsorption occurred. In comparison, photocatalytic treatment of POME by WO_3 NPs under UV light reduced the COD value more efficiently than photolysis and adsorption. A catalyst that loaded with 0.5 g/L WO_3 achieved highest photodegradation after 240 min of UV-irradiation with 51.15 % COD removal. For longevity study of WO_3, photocatalytic degradation of POME was reached 84.70% after 16 hours of photocatalytic treatment.

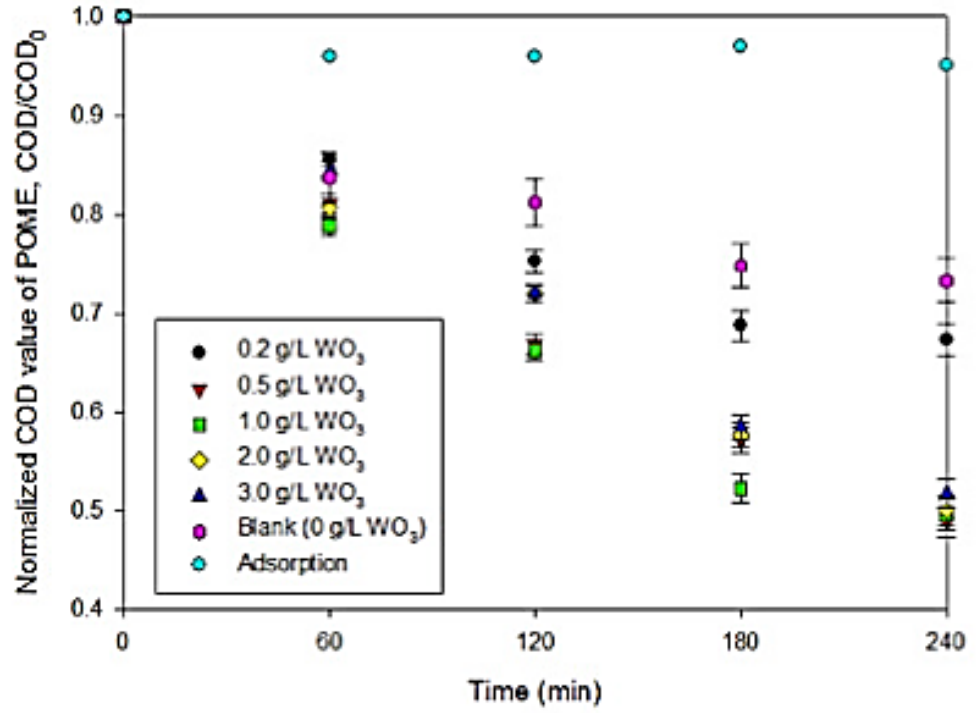

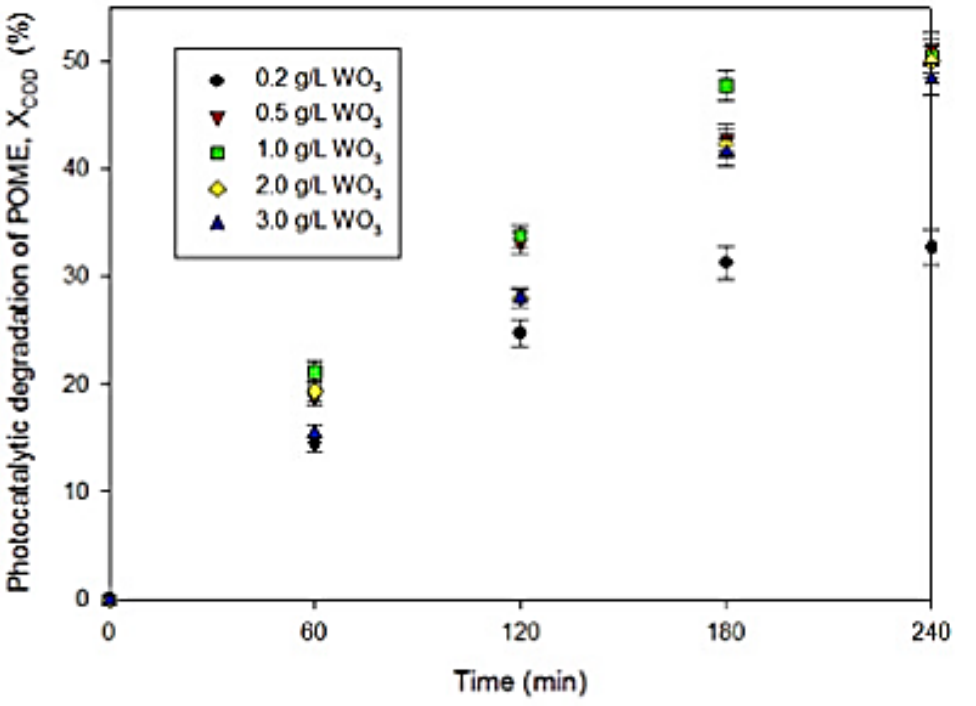

Figure 2.21: (a) Normalized COD and (b) Photocatalytic degradation (Cheng et al., 2021).

CHAPTER 3

METHODOLOGY

3.1 Chemicals and materials

Lemon (*Citrus limon*) was purchased from a local market in Kampar. Copper (II) nitrate trihydrate, $Cu(NO_3)_2.3H_2O$ was purchased from Quality Reagent Chemical, QR&C, New Zealand. The POME sample was collected from a local palm oil mill located in Selangor. All glassware was cleaned with DI water and dried in an oven before use.

3.2 Green synthesis of CuO NPs

3.2.1 Preparation of lemon peel extract (LPE)

Copper(II) oxide nanoparticles were green-synthesized by using lemon peel as a natural source for reducing agents as well as stabilizing agents. The schematic diagram for the preparation of lemon peel extract was presented in Figure 3.1. Firstly, 100 g of lemon peels were washed with DI water to remove the impurities. Washed lemon peels were wiped to dry and cut into small pieces and mixed with 150 mL of DI water. Then, it was heated at 70 °C-80 °C for 20 minutes to extract the phytochemicals in lemon peels, which acts as reducing

and capping agent. Then, the resulting extract was filtered twice by using Whatman No. 1 filter paper and kept at 4 ℃ for further processing.

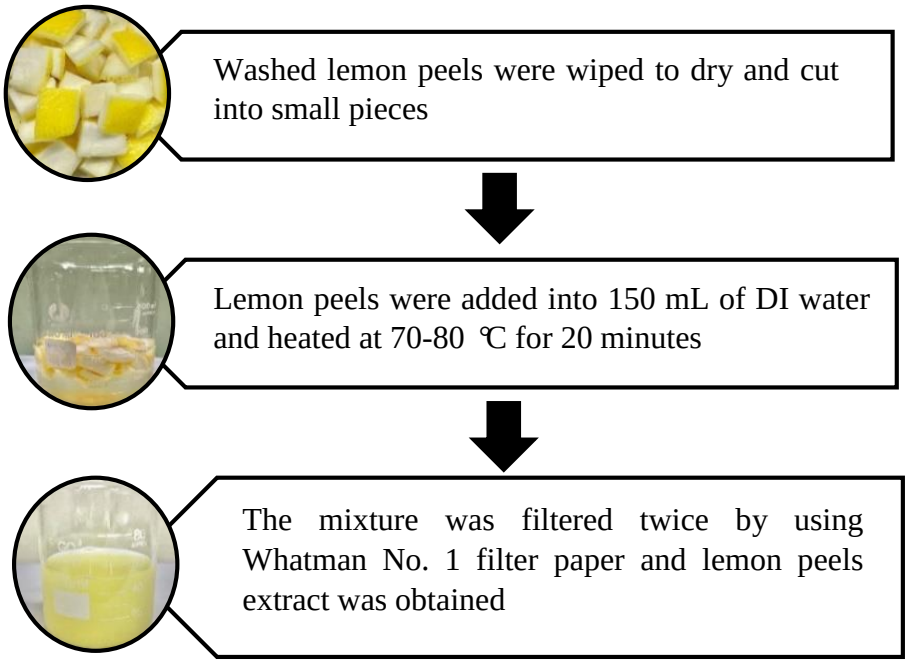

Figure 3.1: Preparation of lemon peel extract.

3.2.2 Green synthesis process of CuO NPs

Volume of 50 mL of aqueous extract of lemon peel was heated at 70-80 ℃ under constant stirring. Then, 2 g of copper(II) nitrate trihydrate was added slowly into LPE. The resultant mixture was heated until a dark green paste was formed. The dark green paste was transferred into crucible and subjected to calcination in a furnace at 450 ℃ for 2 hours. Black colour powder was obtained and characterized by UV-visible spectroscopy (UV-vis), fourier transform infrared spectroscopy (FT-IR), X-ray diffraction (XRD), energy dispersive X-ray

spectroscopy (EDX), scanning electron microscopy (SEM), and transmission electron microscopy (TEM).

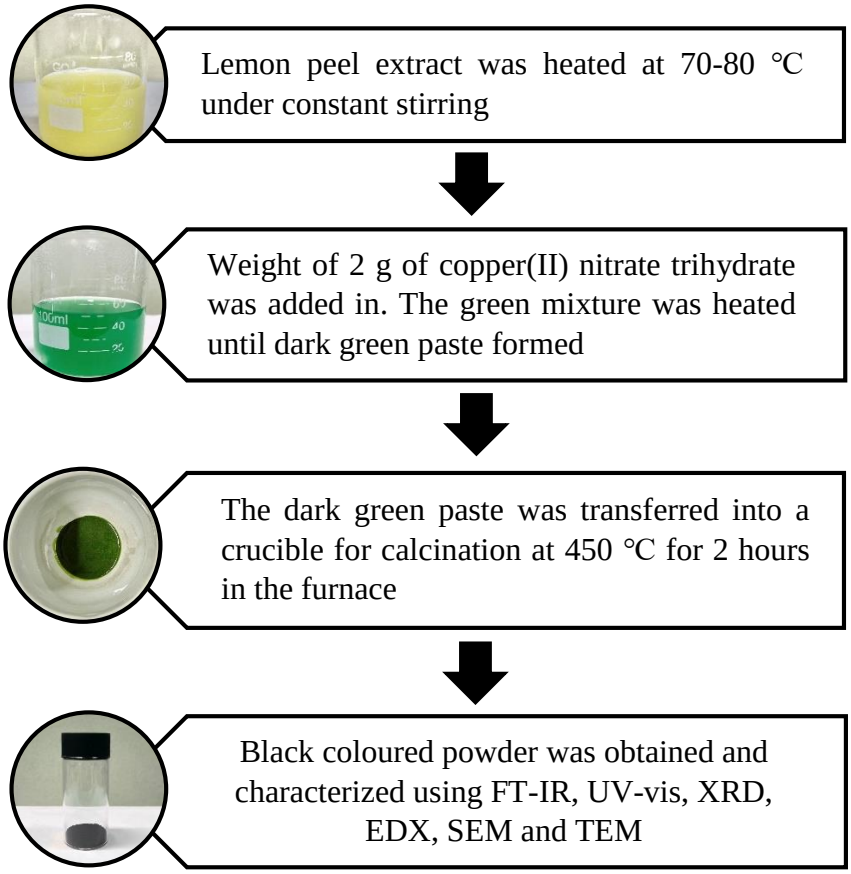

Figure 3.2: Green synthesis process of CuO NPs using lemon peel extract.

3.3 Characterization of green-synthesized CuO NPs

The synthesized CuO NPs were characterized by UV-visible spectroscopy (UV-vis), fourier transform infrared spectroscopy (FT-IR), X-ray diffraction (XRD), energy dispersive X-ray spectroscopy (EDX), scanning electron microscopy (SEM), and transmission electron microscopy (TEM). The optical absorption

properties of CuO nanoparticles, lemon peel extract and copper(II) nitrate trihydrate were recorded by UV-Vis single beam spectrophotometer (Thermo Scientific GENESYS 10S) in the range of 200-800 nm. Deionized (DI) water was used as blank. Weight of 1.5 mg of green-synthesizing CuO NPs was mixed with 10 mL of DI water and sonicated for 20 minutes to disperse the CuO NPs. FT-IR analysis was used to determine the phytochemicals that exist in the extract, which play the role of reducing and capping in the CuO NPs synthesis. In addition, FT-IR analysis was utilized to determine the functional group for the formation of CuO NPs. The FT-IR spectra of lemon peel extract (LPE) and CuO NPs were measured by KBr pellet method using FTIR spectrophotometer (Perkin Elmer Spectrum RX1) and scanned in 4000-400 cm^{-1} range. Volume of 2 mL of the LPE was freeze dried into solid form before subjected to FT-IR analysis. XRD analysis was utilized to determine the crystal phases and crystallinity of CuO NPs. XRD analysis of synthesized CuO NPs were carried out by using Shimadzu XRD 6000 Cu Kα radiation (λ = 1.5406 Å, Voltage = 40 kV, Current = 30 mA, scan rate of 0.02 s^{-1}, scan range of 2θ from 30-80^{o}). The obtained result was compared to The International Centre for Diffraction Data (ICDD) card No.01-089-5896. Electron-dispersive X-ray spectroscopy, EDX (Oxfords Instrument X-Max Energy Dispersive Diffractometer) was used to examized the elemental composition of CuO NPs. Scanning electron microscopy, SEM (JEOL JSM-6701F) operated at 3.0 kV was used to analysed the surface morphology, shape and average particle size of CuO NPs. Transmission electron microscopy, TEM (JEOL JEM-3010) further determine the particles size and internal morphologies of CuO NPs.

3.4 Calculation of crystallite size using Debye-Scherrer formula

Based on XRD spectra, the average crystallite size of CuO NPs were calculated by using Debye-Scherrer formula as below:

$$D = \frac{k\lambda}{(\beta \cos\theta)}$$

where

D = Mean size of nanoparticle

k = Scherrer constant, 0.9

λ = X-ray wavelength, (Cu, Kα radiation = 1.5406 × 10^{-10} m)

β = Full width half maximum width (FWHM) of diffraction peak in radian 2θ

θ = Bragg's diffraction angle

β can be calculated by using formula shown below:

$$\beta = \frac{\text{FWHM in } 2\theta \times \pi}{180^\circ}$$

3.5 Calculation of band gap energy

Optical band gap energy (E_g) of synthesized CuO NPs can be found using a Tauc plot. The Tauc equation is shown below:

$$\alpha h\nu = \mathrm{D}\,(h\nu - E_g)^n$$

where

α = absorption coefficient

h = Planck's constant, 6.626×10^{-34} Js

ν = Frequency of photon

D = proportionality constant

E_g = band gap energy in eV

n = 0.5 (direct transition) or 2 (indirect transition) of CuO NP

The absorption coefficient, α can be approximated as follows:

$$\alpha \approx 2.303\ \frac{A}{d}$$

where

A = absorbance of the sample

d = thickness of the cuvette, which is 1 cm.

A Tauc plot was created by plotting $(\alpha hv)^n$ against photon energy, hv in eV. The value of n is equal to 0.5 for direct transition and 2 for indirect transition. Based on the Tauc plot, band gap energy of CuO NPs was obtained by extrapolating the best linear region appeared to the x-axis.

3.6 Photocatalytic activity of palm oil mill effluent (POME) by green-synthesized CuO NPs

3.6.1 Preparation of POME

POME was filtered to remove suspended solids using a filtration system as shown in Figure 3.3 (Phang et al., 2021). The filtration system was set up from bottom to top, with 1-part coarse sand, 1-part activated carbon and 3-parts fine sand, as well as a thin layer of cotton at the bottom of the container and in between each sand layer as presented in Figure 3.3. Before filtering the POME through the filtration system, the system was washed with 1 L of 5 % nitric acid (HNO_3) and 4 L of deionized water. Then, the chemical oxygen demand (COD) value of filtered POME was measured.

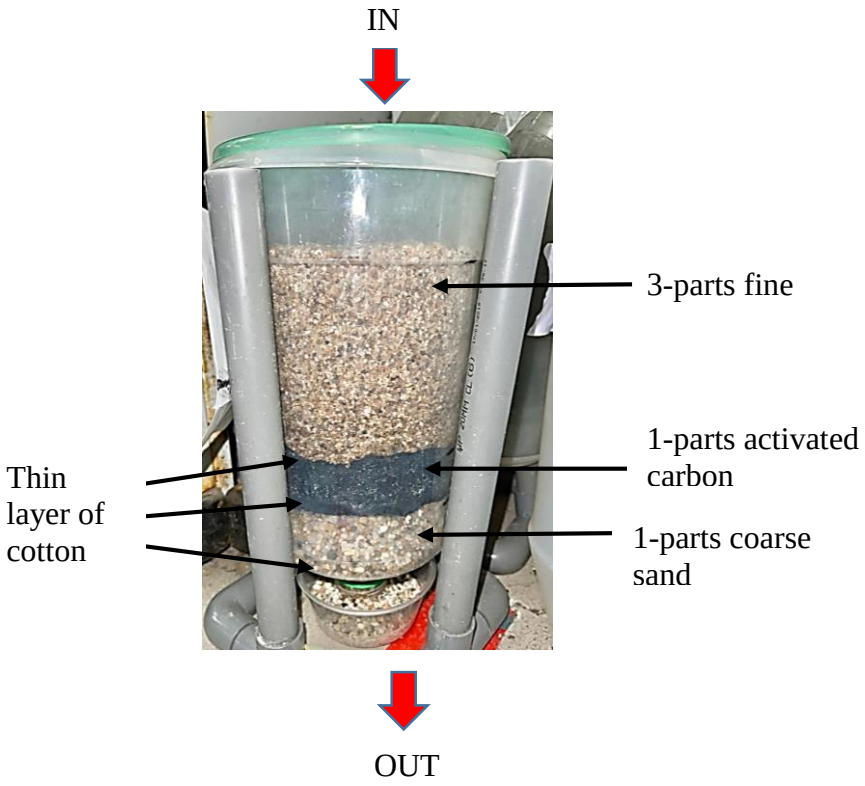

Figure 3.3: Set up of filtration system (Phang et al., 2021).

3.6.2 Photocatalytic degradation of filtered POME using CuO nanoparticles under UV irradiation

In a 500 mL beaker, 150 mL of filtered POME sample was added followed by 75 mg of CuO NPs. The suspension was allowed to stir magnetically in the dark conditions for 30 minutes at room temperature to reach absorption- desorption equilibrium. The suspension was then stirred continuously under an 18 W UV lamp (Roxin, 220-240 V, 50 Hz) for 3 hours. During the 3 hours period, time-based photocatalytic degradation of filtered POME was conducted by removing 10 mL of the POME-CuO NPs suspension before photocatalytic degradation and

every 30 minutes for 3 hours. After 3 hours, the suspension was allowed to centrifuge at 3000 rpm for 15 minutes to remove CuO NPs. Then, 2 mL of supernatant of POME sample (unirradiated and irradiated) was injected into the high-range COD (HACH 2125915 vial digestion solution COD-HR) vial from HACH Company, Germany. The vials were then digested at 150 ℃ for 2 hours using the HACH DRB 200 COD digital reactor. Finally, the COD value of unirradiated and irradiated POME were measured using HACH DR/890 Colorimeter. For comparison, filtered POME sample without the addition of CuO NPs was carried out under similar conditions.

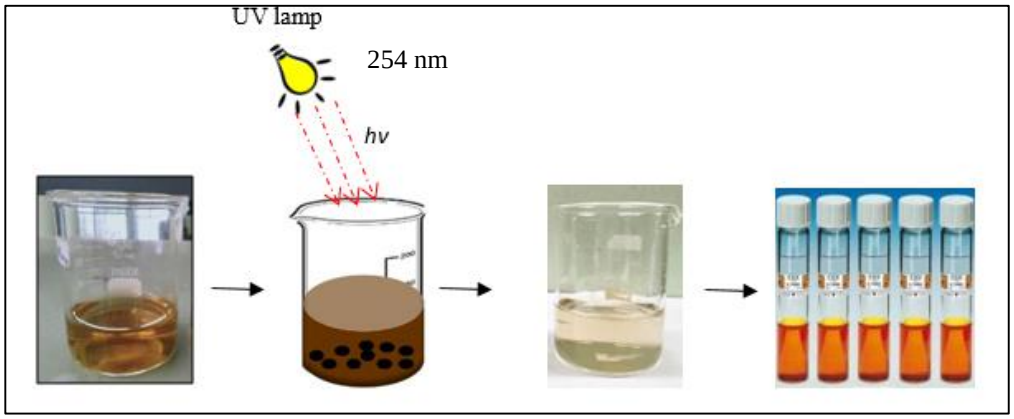

Figure 3.4: Schematic representation of photodegradation of POME under UV light irradiation.

3.6.3 Photocatalytic degradation of filtered POME using CuO nanoparticles under dark condition

In a 500 mL beaker, 150 mL of filtered POME sample was added followed by 75 mg of CuO NPs. The suspension was allowed to stir magnetically in dark conditions for 30 minutes at room temperature to reach absorption- desorption equilibrium. The suspension was then stirred continuously under dark condition in a fully cover box for 3 hours. CuO NPs's photocatalytic activity was conducted by removing 10 mL of the POME-CuO NPs suspension before photocatalytic degradation and every 30 minutes for 3 hours. After 3 hours, the suspension was allowed to centrifuge at 3000 rpm for 15 minutes to remove CuO NPs. Then, 2 mL of supernatant of POME sample was injected into the high-range COD (HACH 2125915 vial digestion solution COD-HR) vial from HACH Company, Germany. The vials were then digested for 2 hours at 150 ℃ using the HACH DRB 200 COD digital reactor. Finally, the COD value of POME were measured using HACH DR/890 Colorimeter.

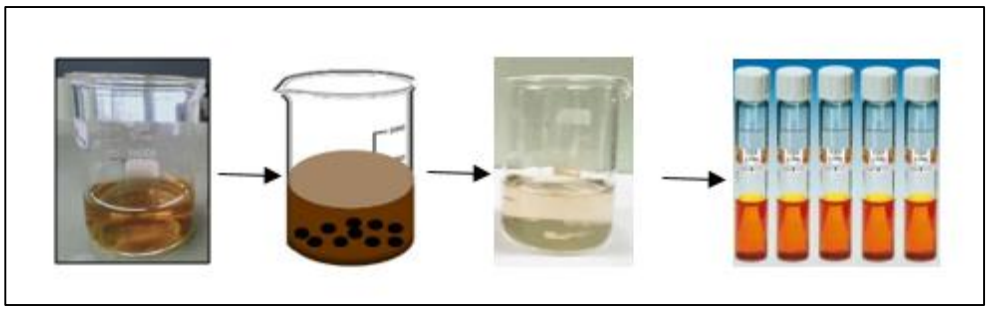

Filtered POME **POME with CuO NPs** **Degraded POME** **COD-HR vial**

Figure 3.5: Schematic representation of degradation of POME under dark condition.

3.6.4 Calculation of COD removal efficiency

The extend of POME degradation was observed by measuring chemical oxygen demand (COD) values. The COD removal's percentage was calculated by the formula as shown below:

$$\text{Percentage of COD removal} = \frac{COD_0 - COD_t}{COD_0}$$

where

COD_0 = Initial COD value of the POME before expose to UV irradiation (mg/L)

COD_t = COD value of the POME after photodegradation at different time interval (mg/L)

3.7 Phytotoxicity evaluation

The phytotoxicity of POME samples before and after photocatalytic degradation were evaluated by using mung bean (*Vigna radiata* L.) seed. Prior to the experiment, the mung bean seeds were sterilized with 0.5 (w/v) % NaOCl solution followed by washed thoroughly with distilled water. After that, cotton pads and 10 mung bean seeds were placed evenly in each sterilized petri dishes. Three different sets of petri dishes were prepared and soaked with 20 mL of tap water (control) and 20 mL each of POME solutions (before and after photodegradation). The petri dishes were placed indoor and replenished with 10 mL of their respective sample at a fixed interval time of 24 h for 7 continuous

days at an ambient temperature. After 7 days, the radicle lengths of *Vigna radiata* L. were measured and the POME samples' phytotoxicity were calculated by the equation below:

$$\text{Phytotoxicity} = \frac{L_c - L_s}{L_c} \; x \; 100\%$$

where

L_c = Control's radical length

L_s = Samples' radical length

CHAPTER 4

RESULTS AND DISCUSSION

4.1 Synthesis of CuO nanoparticles

In this study, CuO NPs were green synthesized using lemon (*Citrus limon*) peel extract (LPE). The bottom-up approach was used in CuO NPs synthesis using copper (II) nitrate trihydrate salt, $Cu(NO_3)_2.3H_2O$ as the metal precursor. The LPE contains various phytochemicals such as alkaloids, flavonoids, quinines, carbohydrates etc. that act as reducing as well as stabilizing agents for green synthesis. LPE was heated at the range of 70-80 ℃ to prevent decomposition of the phytochemicals at higher temperature. $Cu(NO_3)_2.3H_2O$ consists of divalent copper cations (Cu^{2+}) was added into the hot LPE slowly with continuous heating and stirring to make sure the salt dissolved homogeneously and the shape and size of CuO NPs formed more uniformly. During the continuous heating at 70-80 ℃, the colour of solution changed slowly from green to dark green, indicating the formation of copper atoms (Cu^0). A reduction process of Cu^{2+} from metal precursor to Cu^0 by biomolecules in lemon peel extract has occurred. During the growth phase process, Cu^0 rearrange themselves to form Cu^0 complexes. Cu^0 complexes tend to form oxides due to the instability. Cu^0 complexes react with atmospheric oxygen to form CuO NPs. Biomolecules in LPE form bio-capping ligands that prevent agglomeration and oxidation of synthesized nanoparticles (Javed et al., 2020). A dark green paste formed by solvent evaporation was subjected to calcination. Calcination of the paste causes oxygen binding onto remaining Cu^0 complexes, crystallization of CuO NPs and decomposition of

remaining biomolecules or unwanted solvents. Organic component such as C, H, O, and N part that having lower boiling temperature than inorganic CuO will be degraded first during thermal decomposition. Hence, purer CuO NPs were formed.

4.2 Characterization of CuO NPs

After calcination at 450 ℃ for 2 hours in furnace, black colour powder was obtained. The black powder was characterized by UV-visible spectroscopy (UV-vis), fourier transform infrared spectroscopy (FT-IR), X-ray diffraction (XRD), energy dispersive X-ray spectroscopy (EDX), scanning electron microscopy (SEM), and transmission electron microscopy (TEM).

4.2.1 UV-visible spectroscopy

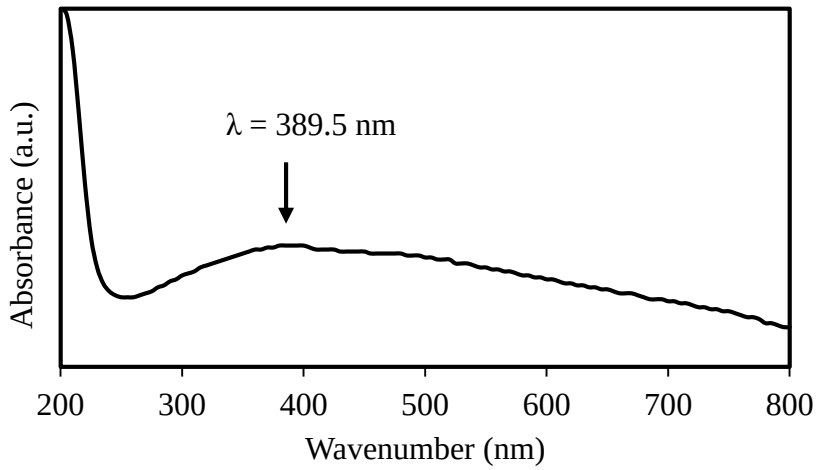

Figure 4.1: UV-vis spectrum of green synthesized CuO NPs.

The UV-vis spectrum was used in determining the optical absorption properties of CuO nanoparticles (Felix et al., 2015). Based on Figure 4.1, the synthesized CuO NPs absorbed at maximum wavelength of 389.5 nm, which has a similar result reported by Thamer et al. (2018), the absorbance peak of UV-vis spectrum that using *Cordia myxa* L. leaves was recorded at 392 nm. The appearance of CuO nanoparticles peak was due to the surface plasmon resonance (SPR) (Apriandanu and Yulizar, 2019). SPR was caused by the collective oscillation of free surface conduction electrons that excited by incident electromagnetic radiation (Phang et al. 2021). Cu^{2+} was reduced to Cu^{0} and rearranged into CuO NPs (Rajgovind et al., 2015).

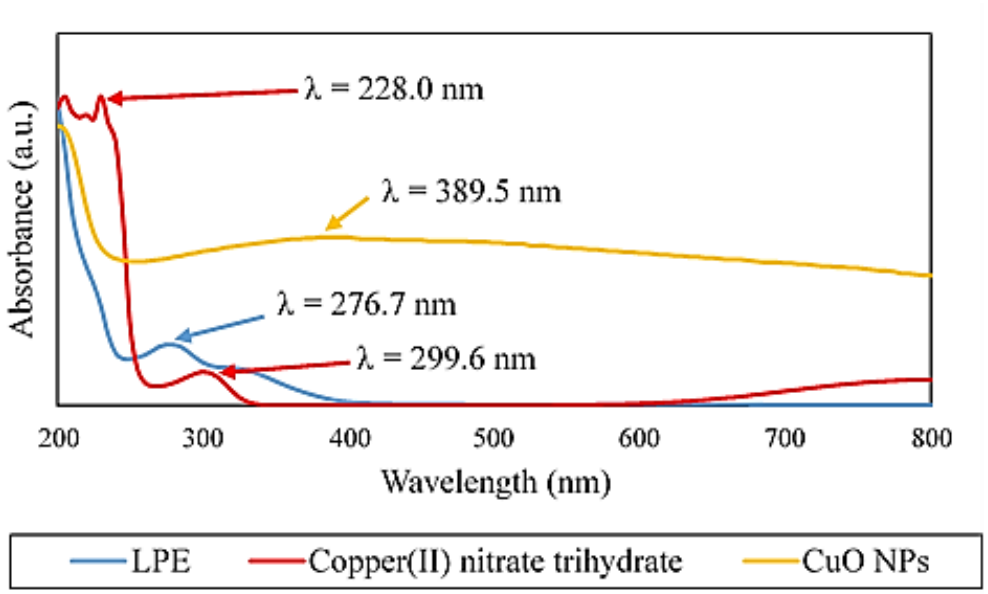

Figure 4.2: UV-vis spectrum of LPE, copper (II) nitrate trihydrate solution and synthesized CuO NPs.

In order to confirm the formation of CuO NPs, UV-vis spectra of CuO NPs, LPE and copper (II) nitrate trihydrate solution were recorded and shown in Figure 4.2. CuO NPs were green synthesized using lemon (*Citrus limon*) peel extract (LPE) that act as reducing as well as stabilizing agents for copper (II) nitrate trihydrate, $Cu(NO_3)_2.3H_2O$ precursor. Based on Figure 4.2, an absorption peak at 276.7 nm was observed in LPE. Krishnaswamy et al. (2019) reported that the peak for lemon extract presented at 288 nm which well agrees with our absorption peak. The absorbance was due to the presence of phytochemicals such as tannins, flavonoids, terpenoids and phenols that in the lemon peel extract. For copper (II) nitrate trihydrate precursor, the absorption peaks shown at 228.0 nm and 299.6 nm. Annealing of the paste was perform to produce the most stable crystalline copper (II) oxide nanoparticles. CuO NPs absorbed at maximum wavelength of 389.5 nm, revealing CuO NPs have been formed.

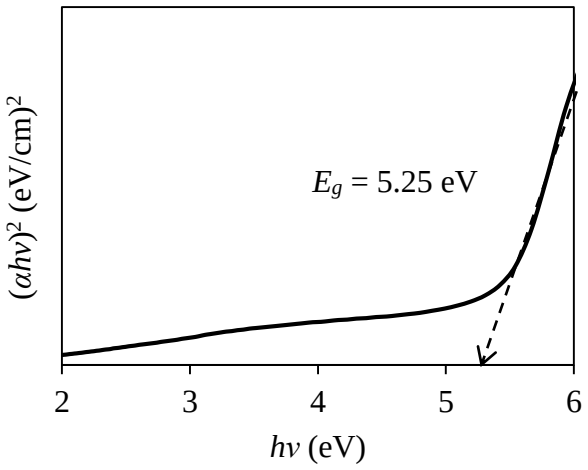

Figure 4.3: Tauc's plot for direct transition in CuO NPs.

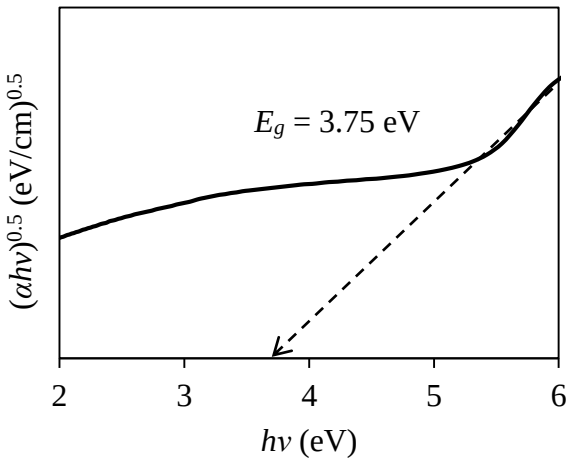

Figure 4.4: Tauc's plot for indirect transition in CuO NPs.

Direct and indirect band gap energies (E_g) of CuO NPs were determined from Tauc plots by extrapolating the linear curves to the photon energy axis. Direct and indirect band gap energies (E_g) of CuO NPs were 5.25 and 3.75 eV respectively, as shown in Figure 4.3 and 4.4. These value were much higher than that of bulk CuO, 3.5 eV and 1.2 eV respectively. The blue shift behavior occurred due to quantum confinement effects, which resulting from the decreasing of nanoparticle size. Photon on a semiconductor will only be absorbed when the minimum energy of it is sufficient to promote an electron in the valence band to conduction band. The synthesized CuO NPs are highly confined and have structured absorption spectrum due to the changing of its electronic band structure to molecular level with non-vanishing energy spacing. Therefore, the CuO NPs need more energy for transitioning of electron to conduction band from valence band. Thus, CuO nanoparticles have higher band gap energy than the bulk CuO (Koshy and George, 2015). The value of direct band gap energy was larger than the indirect band gap energy, thus CuO NPs are crystalline in nature (Radhakrisknan and Beena, 2014).

4.2.2 Fourier transform infrared spectroscopy (FT-IR)

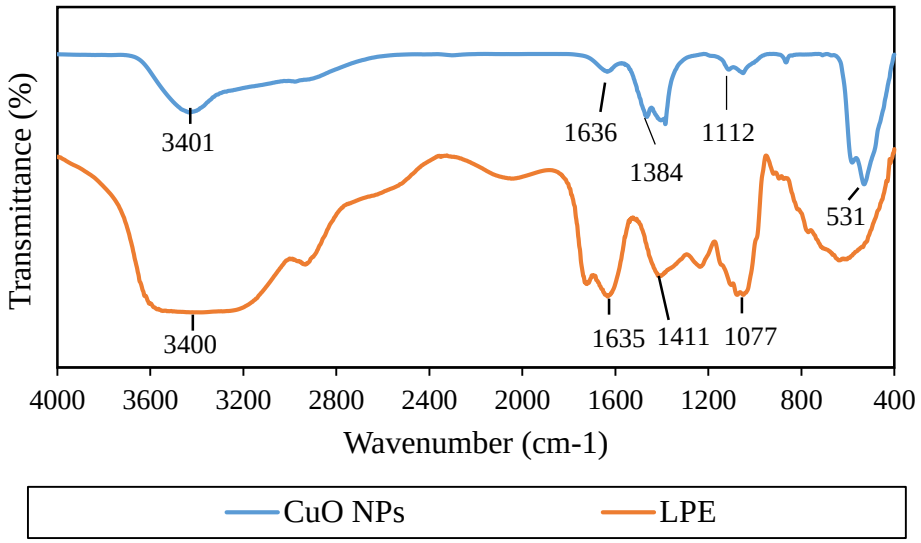

Figure 4.5: FTIR spectra of green synthesized CuO NPs and LPE.

Fourier transform infrared spectroscopy measurement was carried out to determine the phytochemicals that presented in the extract, which functioned as reducing and capping agent in the CuO nanoparticle synthesis. Besides, FTIR spectrum was used to determine the Cu-O bond. The FTIR spectra was analysed in the region between 4000-400 cm^{-1}. Based on Figure 4.5, the FTIR spectrum of CuO NPs showed a sharp and intense peak at 531 cm^{-1} that represented to Cu-O stretching vibration confirming the formation of CuO NPs, which in accordance with the finding by Phang et al. (2021). The peaks at 3401 cm^{-1} was assigned to the O-H stretching vibration (Manyasree et al., 2017). Peaks occurred at 1636 cm^{-1} and 1384 cm^{-1} attributed respectively to the C=O stretching vibration of carboxylic acid and O-H bending of phenolic group (Apriandanu and Yulizar, 2019). The peak occurred at 1112 cm^{-1} confirmed the

C-O symmetric stretching vibration, which is similar to the work of Kannan et al. (2020). Roguai and Djelloul (2021) reported that the absorption spectral of Cu(I)-O vibration was in the range 605-600 cm^{-1}. However, there is no absorption peak observed in these range in the CuO NPs spectrum, so it can confirm that there is no existence of Cu_2O phase in the green-synthesized CuO NPs.

Table 4.1: A comparison of peak assignment of the synthesized CuO NPs from the literature review.

Wavenumber (cm^{-1})	Peak assignment	Wavenumber from literature review (cm^{-1})
3401	O-H stretching vibration	3398 (Manyasree et al., 2017)
1636	CO stretching vibration of carboxylic acid	1602 (Apriandanu and Yulizar, 2019)
1384	O-H bending of phenolic group	1384 (Phang et al., 2021)
1112	C-O symmetric stretching vibration	1114 (Kannan et al., 2020)
531	Cu-O stretching vibration	532 (Phang et al., 2021)

Based on the FTIR spectrum of lemon peel extract (LPE), a broad and intense peak at 3400 cm^{-1} represented the O-H groups of phenols, alcohols and carboxylic acids that found in cellulose, pectin and lignin. Stretching vibration of carboxylate ions (COO-) was shown at peak around 1635 cm^{-1}. Absorption peak at 1411 cm^{-1} represented the HCH and OCH vibration of cellulose. Sabanovic et al. (2020) reported that the absorption peak at 1077 cm^{-1} indicated the C-O stretching vibration.

Table 4.2: A comparison of peak assignment of the lemon peel extract from the literature review.

Wavenumber (cm^{-1})	Peak assignment	Wavenumber from literature review (cm^{-1})
3400	O-H stretching vibration	3387 (Al-Qaisi et al., 2018)
1635	COO^- stretching vibration	1622 (Sabanovic et al., 2020)
1411	HCH and OCH in plane bending vibration	1423 (Sabanovic et al., 2020)
1077	C-O stretching vibration	1020 (Sabanovic et al., 2020)

To understand better about the CuO NPs formation, the FTIR spectra of CuO NPs and lemon peel extract (LPE) were compared. The FTIR spectrum of CuO NPs showed a sharp and intense band at 531 cm^{-1} that represented to Cu (II)-O bond confirming the formation of CuO NPs, which was not observed in LPE.

Some peaks in the IR spectrum of CuO NPs were shifted to higher frequencies compared to LPE spectrum, from 3400 to 3401, 1635 to 1636, 1077 to 1112 cm^{-1}, which corresponds to the carbonyl and hydroxyl groups. FTIR studies introduced that the hydroxyl and carbonyl groups can bind to the metal stronger and coat over the nanoparticles to stabilize the NPs to prevent aggregation (Ganapuram et al., 2015). The absorption bands other than the Cu-O band in the FTIR spectra of CuO NPs appeared in the FTIR spectra of the LPE (Figure 4.5), indicating that the functional groups on the CuO NPs are from the lemon peel extract. Finally, cellulose, pectin and lignin, etc. are found to play the role of reducing and stabilizing agent in CuO NPs synthesizing.

4.2.3 X-ray diffraction (XRD)

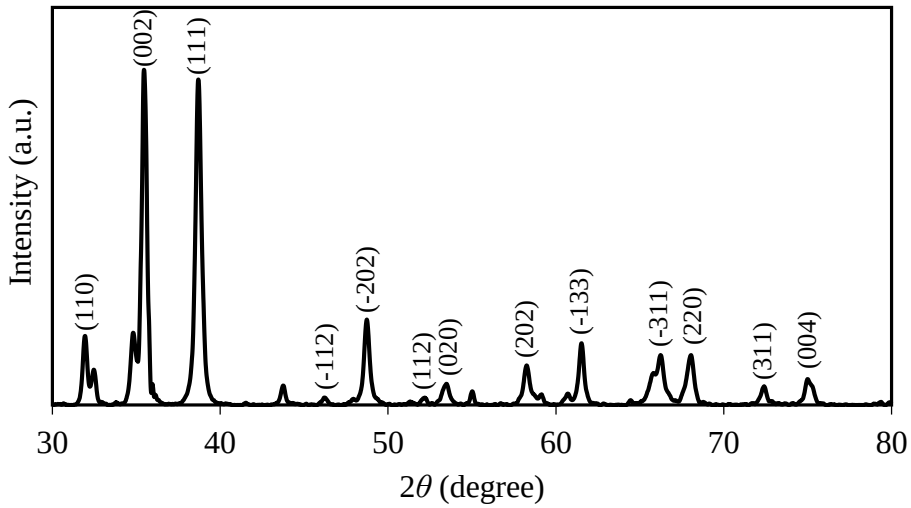

Figure 4.6: XRD diffractogram of CuO NPs.

The crystal phases and crystallinity of CuO NPs were evaluated by XRD. Peak intensity indicates the position of atoms within the lattice structure, while peak width defines the crystalline size of nanoparticles. The Miller indices (*hkl*) identify the crystallographic plane (Ohring, 1995). Figure 4.6 shows the XRD spectrum of synthesized CuO NPs. The specific diffraction peaks at 2θ of 32.15 °, 35.69 °, 38.92 °, 43.97 °, 48.95 °, 53.62 °, 55.22 °, 58.42 °, 61.74 °, 66.44 °, 68.20 °, 75.14 ° and 75.42 ° were indexed to (110), (002), (111), (-112), (-202), (112), (020), (202), (-133), (-311), (220), (311) and (004) crystal planes respectively. These diffraction peaks were agreed well with the standard card of The International Centre for Diffraction Data (ICDD) card No.01-089-5896, confirming the monoclinic phase CuO NPs. The presence of intense peaks revealed the CuO NPs were in crystalline nature. The similar work was reported

by Sathishkumar et al. (2020) where the diffraction peaks were located at 32.55 °, 35.58 °, 38.75 °, 48.84 °, 53.50 °, 58.36 °, 61.58 °, 68.09 ° are indexed to (110), (-111), (111), (-202), (020), (202), (-113) and (220) respectively. The degree of crystallinity of the synthesized CuO NPs acquired was 17.73 % and this may be due to broadening of the peaks in diffractogram and the large amount of amorphous content. The CuO NPs' crystalline size was calculated by Debye Scherrer equation. The crystalline size of the highest diffraction peak at 35.48 ° in radian 2θ, was calculated to be 23.37 nm as presented in Appendix A.

4.2.4 Energy-dispersive X-ray spectroscopy (EDX)

(a)

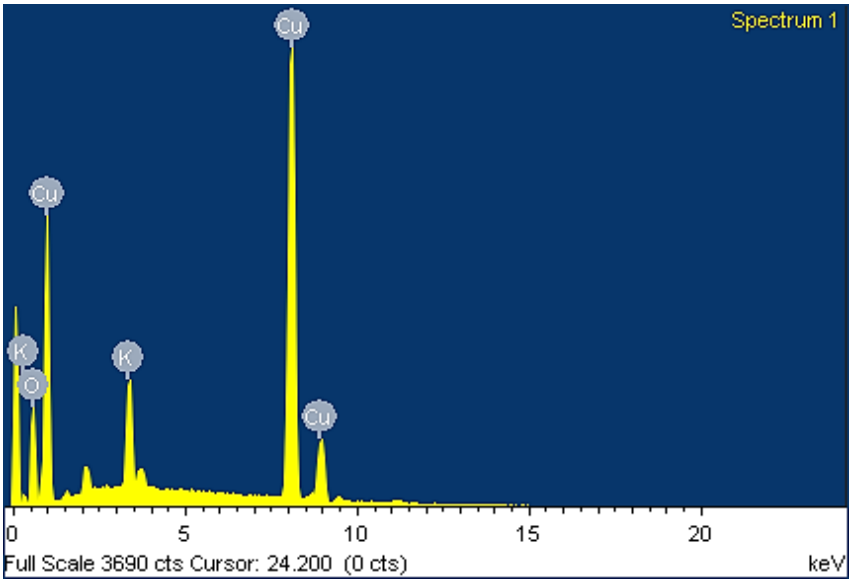

(b)

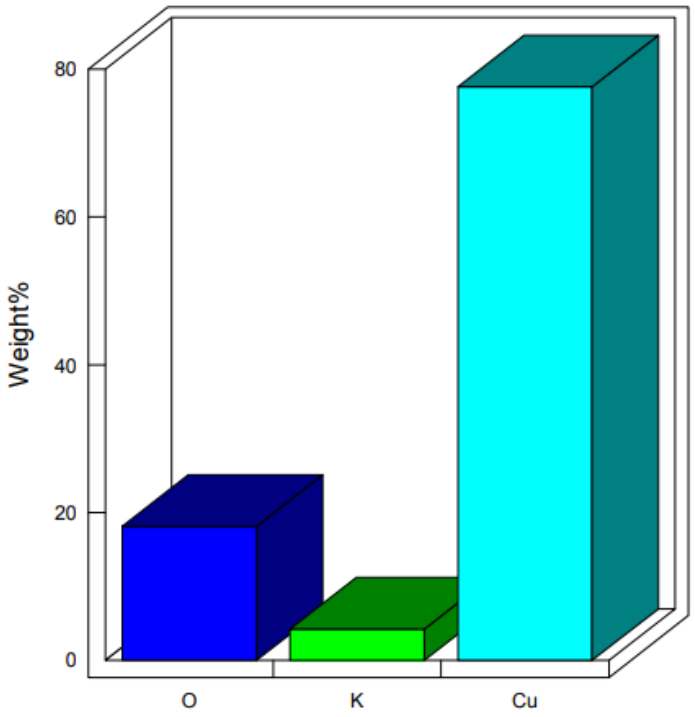

Figure 4.7: (a) EDX spectrum and (b) weight percent distribution histogram of green-synthesized CuO NPs.

EDX analysis was carried out to determine the chemical composition of synthesized CuO NPs. EDX spectrum shows that the synthesized CuO NPs contain element of copper, oxygen and potassium. Based on the weight percent distribution histogram of green synthesized CuO NPs, the weight percent of copper (Cu), oxygen (O), and potassium (K) were found to be 77.61 %, 18.14 % and 4.25 % respectively. The presence of strong signals of Cu and O elements indicates the successful formation of CuO NPs. Traces of potassium came from aqueous extract of lemon peels. To obtain CuO NPs with higher purity, the synthesized CuO NPs can be washed with deionized water to eliminate trace of potassium.

4.2.5 Scanning electron microscopy (SEM)

(a)

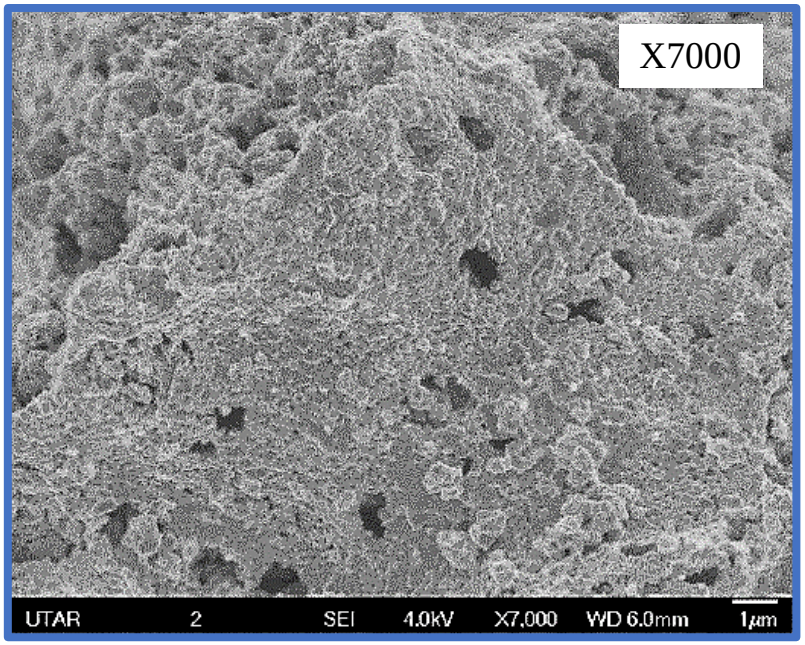

(b)

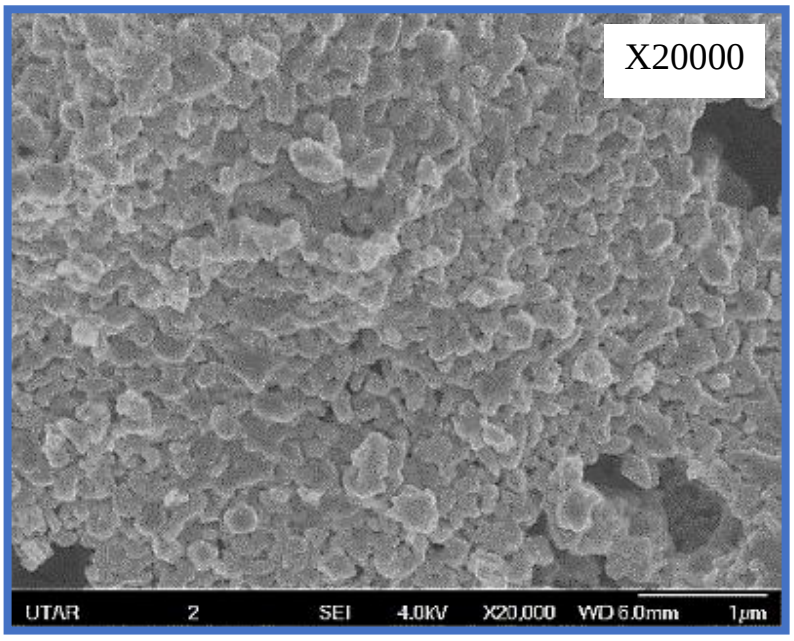

Figure 4.8: SEM image of synthesized CuO NPs with magnification of (a) x7000 and (b) x20000.

(c)

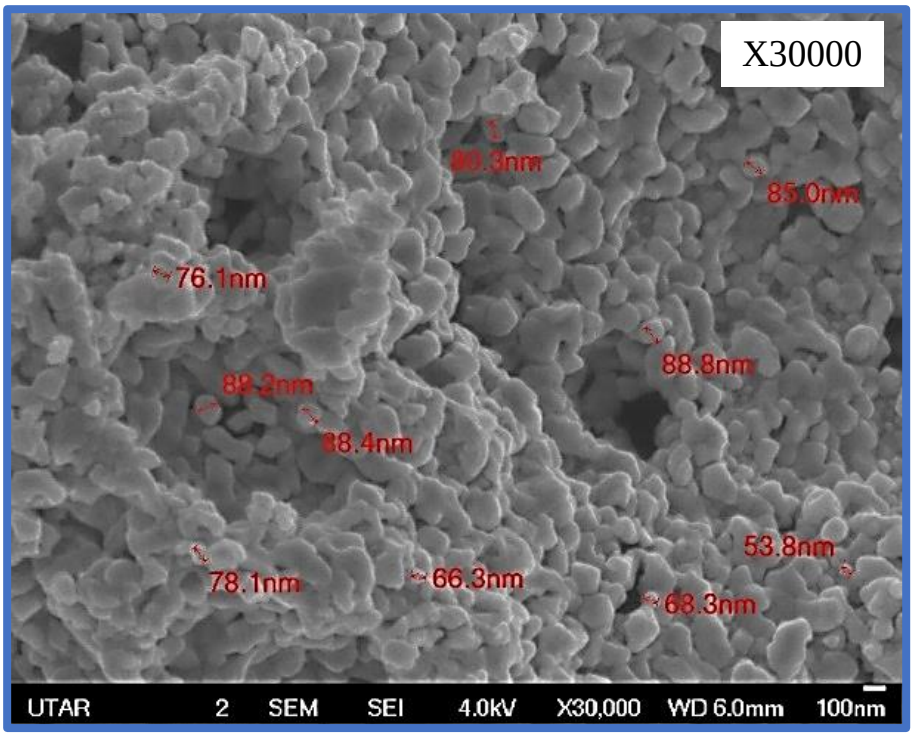

Figure 4.9: SEM image of synthesized CuO NPs with magnification of (c) x30000.

Scanning electron microscope was used to determine the surface morphological of CuO NPs. Figure 4.8 (a) and (b) showed that the synthesized CuO NPs were agglomerated spherical in shape. The average particle size of CuO NPs measured from SEM was 77 nm as shown in Figure 4.9 (c).

4.2.6 Transmission electron microscopy (TEM)

(a)

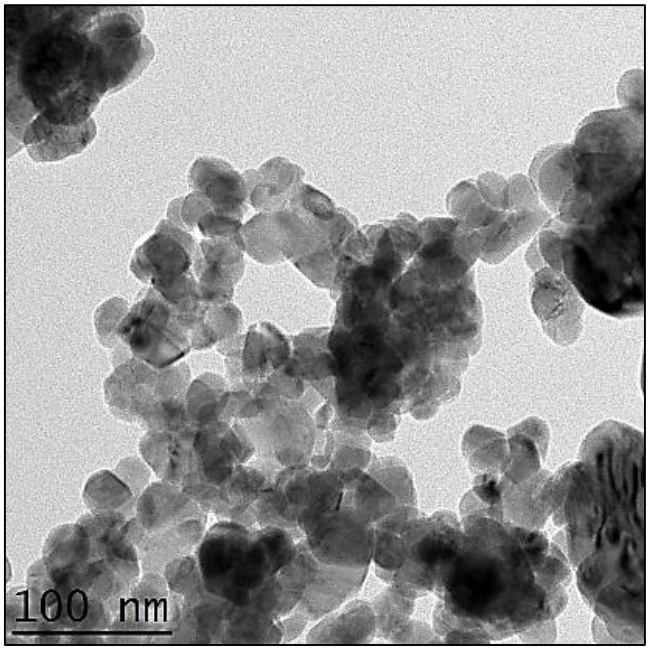

(b)

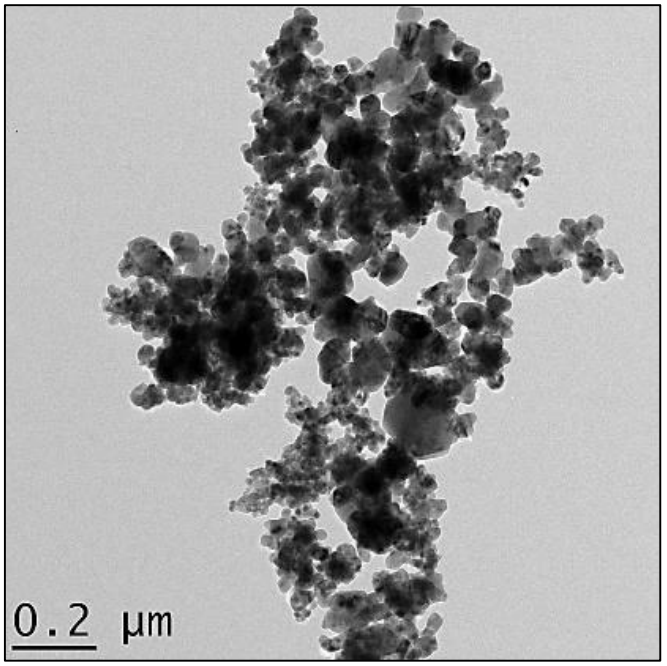

Figure 4.10: TEM images of CuO NPs taken at (a) 100 nm and (b) 0.2 µm.

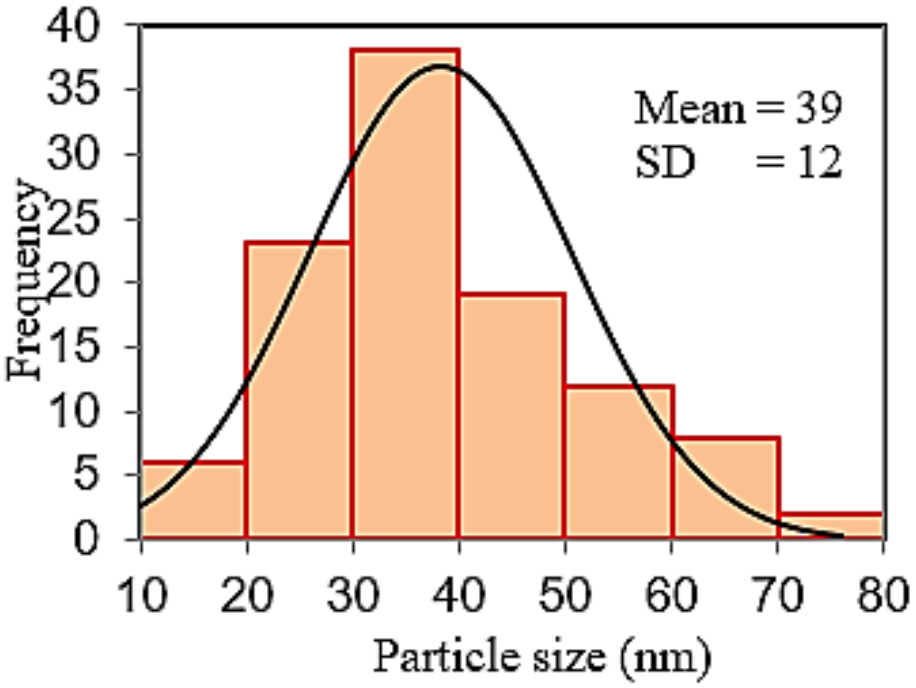

Figure 4.11: Histogram of particle size distribution of green-synthesized CuO NPs.

TEM is effective and has a higher resolution, allowing it to examine the internal structure of nanoparticles, contributing information on the morphology and size distribution of nanoparticles (Patel et al., 2022). TEM images showed the spherical shape of CuO NPs, which is agreed with the image formed by SEM. The CuO NPs had an average particle size of 39 nm in diameter as shown in Figure 4.11.

Table 4.3: A comparison of lemon peel extract-derived CuO NPs with other biosynthesized CuO NPs reported in the literature.

Plant material	Size (nm)	Shape	References
Aloe vera (leaves extract)	5-20	Spherical	(Sharma and Kumar, 2020)
Caesalpinia bonducella (seed extract)	13	Rice-shaped	(Sukumar et al., 2020)
Carica papaya L. (peel extract)	85-140	Agglomerated spherical	(Phang et al., 2021)
Cavendish banana (peel extract)	50-85	Agglomerated spherical	(Aminuzzaman et al., 2017)
Opuntia focus-indica (peel extract)	20-60	Spherical	(Badri et al., 2021)
Stachys lavandulifolia (flower extract)	20-35	Agglomerated spherical	(Veisi et al., 2021)
Tamarindus indica L. (leaves extract)	50-100	Spherical	(Zaman et al., 2020)
Tinospora crispa (leaves extract)	10-40	Rice-shaped	(Apriandanu and Yulizar, 2019)
Triticum aestivum (seed extract)	21-42	Spherical	(Buazar et al., 2019)
Citrus limon (peel extract)	77	Agglomerated spherical	Current work

4.3 Evaluation of photocatalytic activity of CuO NPs

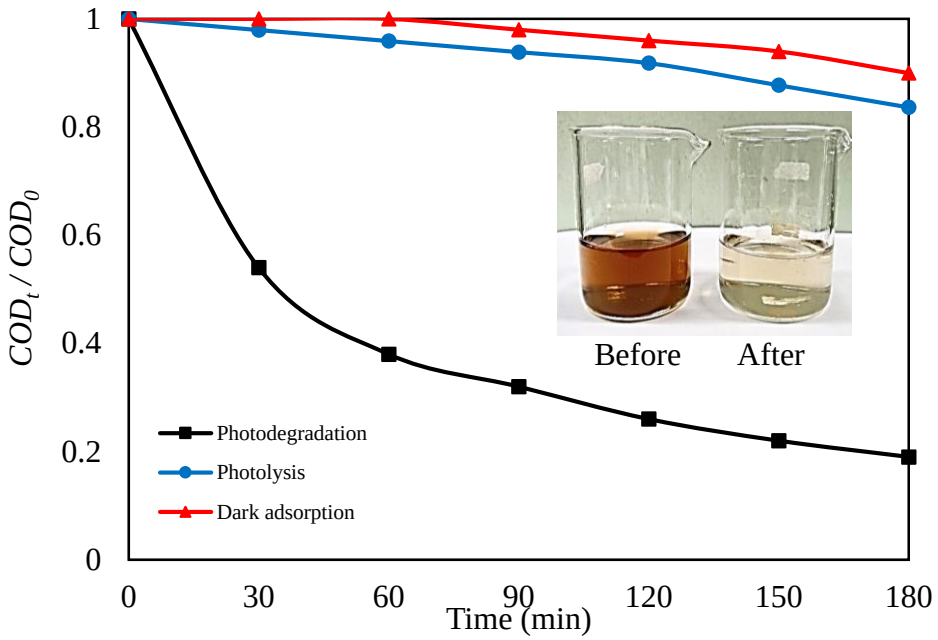

Figure 4.12: Photocatalytic degradation of palm oil mill effluent (POME) by CuO NPs at different experimental conditions. The inset shows the POME's colour before and after exposure to UV irradiation.

In this study, the CuO NPs' photocatalytic activity was evaluated by the degradation of palm oil mill effluent (POME) under UV irradiation, and the extend of POME degradation was observed by measuring chemical oxygen demand (COD) values. The photocatalyst used in the heterogeneous photocatalytic treatment of POME was lemon peel extract mediated CuO NPs. The POME sample was also exposed to direct UV light without the photocatalyst to perform a blank analysis. The blank was employed as a control and to demonstrate the utility of CuO NPs as a role of photocatalyst in the degradation of POME in this study. The degrading activities of CuO NPs are depicted in

Figure 4.12 under various experimental circumstances. The adsorption of organic matter such as carbohydrates, amino acids, lignin, phenolic, and other compounds within POME on the surface of CuO NPs under dark conditions for 3 hours resulted in a reduction of about 10 % COD. For photolysis case, the POME was irradiated under UV light without the presence of CuO NPs, and after 3 hours, the COD was reduced by around 17 %, demonstrating that POME solution has a high resistance to UV irradiation. In the presence of CuO NPs, however, after 3 hours of UV light irradiation, roughly 81 % of COD was reduced, and this reduction in COD was achieved by the destruction of the soluble protein and carbohydrate in POME. High reduction in COD value indicates high reduction of organic pollutant in the POME. In the inset of Figure 4.12, the appearance of the POME solution is also depicted. The POME was in dark brown colour before UV irradiation, however after 3 hours of UV light irradiation, the POME turned pale yellow due to photocatalytic degradation of POME.

CuO NP is a semiconductor that can generate electron-hole pairs (e^-/h^+) as a result of transitioning excited electrons to the conduction band from the valence band and forming holes in the valence band after absorbing photon energy ($h\nu$) from UV light (Equation (1)). The oxygen and water molecules in the POME reacted with the electron-hole pairs and created the hydroxyl radical (OH•), which broke down the organic complex in the POME. Oxygen (O_2) interacted with excited electrons (e-) and dissociated hydrogen ions (H^+) from water molecules to generate hydrogen peroxide (H_2O_2) under UV irradiation. (Equation (2)) Hydrogen peroxide was then reduced to hydroxyl radicals and

hydroxide ions (Equation (3)). The organic components in the POME were degraded by hydroxyl radicals into simple, innocuous degradation products. Water, carbon dioxide, methane gas, and other simple molecules were the end products of the photocatalytic degradation process (Equation (4)). A similar work of the photocatalytic degradation of organic contaminants in aqueous medium using CuO nanoparticles has been reported by Phang et al. (2021). The photocatalytic degradation mechanism of POME using green-synthesised CuO NPs is shown in Figure 4.13.

$$\text{CuO NPs} + h\nu\ (\text{UV light}) \rightarrow \text{CuO NPs}\ (e^- + h^+) \quad (1)$$

$$2e^- + O_2 + 2\,H^+ \rightarrow H_2O_2 \quad (2)$$

$$e^- + H_2O_2 \rightarrow OH\bullet + OH^- \quad (3)$$

$$OH\bullet + \text{POME} \rightarrow \text{intermediates} \rightarrow H_2O + CO_2 + CH_4 \quad (4)$$

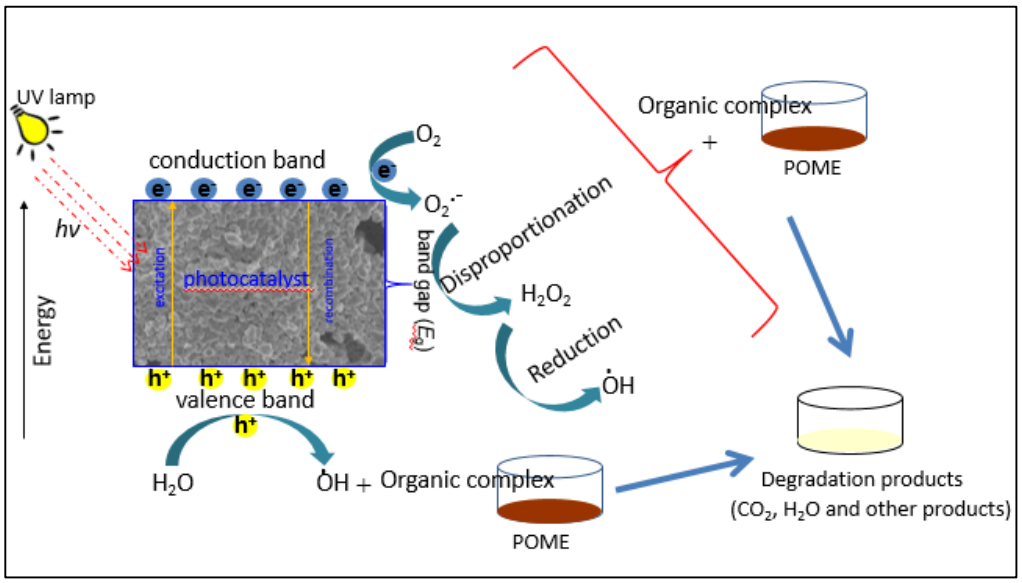

Figure 4.13: Photocatalytic degradation mechanism of POME using green-synthesised CuO NPs (Phang et al., 2021).

Table 4.4: A comparison of photocatalytic performance of CuO nanoparticles on the degradation of various organic pollutants reported in the literature.

Precursor used	**Pollutant**	**Irridiation source**	**Time (min)**	**Efficiency (%)**	**References**
$CuCl_2.2H_2O$	Rhodamine B	UV light	120	65.0	(Zaman et al., 2020)
$Cu(NO_3)_2.3H_2O$	POME	UV light	180	66.0	(Phang et al., 2021)
$CuSO_4 \cdot 5H_2O$	4-Nitrophenol	UV light	20	99.5	(Buazar et al., 2019)
$Cu(NO_3)_2.3H_2O$	Congo red	Sunlight	60	90.0	(Aminuzzaman et al., 2017)
$Cu(CH_3COO)_2H_2O$	Methyl orange	UV light	24	96.0	(Sharma and Kumar, 2020)
$Cu(CH_3COO)_2.H_2O$	Methylene blue	Sunlight	120	98.0	(Kannan et al., 2020)
$Cu(NO_3)_2.3H_2O$	POME	UV light	180	81.0	Current work

4.4 Evaluation of phytotoxicity of POME on *Vigna radiata* L.

(a)

(b)

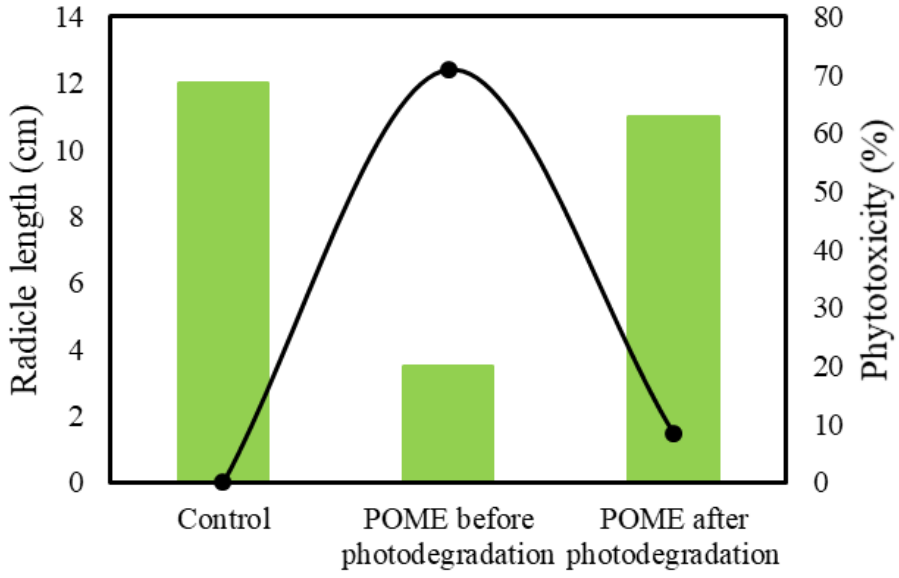

Figure 4.14: (A) Photograph of *Vigna radiata* L. germination in the sample: 1. control, 2. before degradation, 3. after degradation; (B) Phytotoxicity of POME before and after photodegradation.

Phytotoxicity test was carried out to determine the possible usage of treated POME for irrigation purpose and its environment impact (Chai et al., 2019). The phytotoxicity of POME samples were evaluated by using mung bean (*Vigna radiata* L.) seed on the POME samples before and after photocatalytic degradation. The average radicle length of mung bean seed in tap water, untreated POME solution and photo-treated POME solution were 12 cm, 3.5 cm and 11 cm respectively. Mung bean radicle length suggested a decrease in phytotoxicity in photo-treated POME solution. The phytotoxicity of untreated POME solution was 70.8 %, which strongly inhibited the germination of mung bean seed when compared to tap water (control). When mung bean seed was exposed to the photo-treated POME solution, the phytotoxicity level decreased dramatically to 8.3 %. These findings suggest that green-synthesised CuO NPs show good photocatalytic activity for reducing phytotoxicity in POME.

CHAPTER 5

CONCLUSION

In this study, CuO NPs have been synthesized successfully using aqueous extract of lemon (*Citrus limon*) peels as reducing agent as well as stabilizing agent. The green-synthesized CuO NPs were characterized by UV-vis, FT-IR, XRD, EDX, SEM and TEM. Direct and indirect band gap energies (E_g) of CuO NPs that calculated from Tauc plots were 5.25 and 3.75 eV respectively. The XRD diffractogram showed CuO NPs has monoclinic phase with crystalline nature and average crystalline size of 23.37 nm. SEM result showed the spherically shape CuO NPs have average particle size of 77 nm while 39 nm in diameter based on TEM result. Furthermore, lemon peel extract mediated CuO NPs showed improved photocatalytic activity under irradiation of UV light. The photocatalytic activity of CuO NPs was evaluated by the degradation of palm oil mill effluent (POME) under UV irradiation. The degradation efficiency was obtained 81 % in 3 hours duration under UV irradiation. Green-synthesised CuO NPs show good photocatalytic activity by reducing phytotoxicity in POME by 91.7 %. These investigations clearly shown that the green-synthesized CuO NPs can be used as an efficient photocatalyst for the treatment of POME.

The photodegradation of POME can be further studied by changing the different parameters used such as concentration of POME, amount of CuO NPs, pH of solution, temperature of reaction medium and time of irradiation of light.

REFERENCES

Abdurahman, N.H., Rosli, Y.M. and Azhar, N.H., 2013. The performance evaluation of anaerobic methods for palm oil mill effluent (POME) treatment: a review. In: Quinn, N.W. (eds.). *International Perspectives on Water Quality Management and Pollutant Control*. London: IntechOpen., pp. 86-105.

Alhalili, Z., 2022. Green synthesis of copper oxide nanoparticles CuO NPs from *Eucalyptus globoulus* leaf extract: adsorption and design of experiments. *Arabian Journal of Chemistry*, 15 (5).

Ali, A.S., 2020. Application of nanomaterials in environmental improvement. In: Sen, M. (eds.). *Nanotechnology and the Environment*. London: IntechOpen.

Al-Qaisi, M.Q., Faisal, L.M.A., Al-Sharify, Z.T. and Al-Sharify, T.A., 2018. Possibility of utilizing from lemon peel as a sorbent in removing of contaminant such as copper ions from simulated aqueous solution. *International Journal of Civil Engineering and Technology*, 9 (11), pp. 571-579.

Amin, F. et al., 2021. Green synthesis of copper oxide nanoparticles using *Aerva javanica* leaf extract and their characterization and investigation of *in vitro* antimicrobial potential and cytotoxic activities. *Evidence-Based Complementary and Alternative Medicine*, 2021 (5), pp. 1-12.

Aminuzzaman, M., Kei, L.M. and Liang, W.H., 2017. Green synthesis of copper oxide (CuO) nanoparticles using banana peel extract and their photocatalytic activities. *AIP Conference Proceedings*, 1828 (1).

Anastas, P.T. and Warner, J.C., 1998. *Principles of green chemistry* [Online]. Available at: https://greenchemistry.yale.edu/about/principles-green-chemistry [Accessed: 14 March 2022]

Apriandanu, D.O.B. and Yulizar, Y., 2019. *Tinospora crispa* leaves extract for the simple preparation method of CuO nanoparticles and its characterization. *Nano-Structures & Nano-Objects*, 20.

Badri, A., Slimi, S., Guergueb, M., Kahri, H. and Mateos, X., 2021. Green synthesis of copper oxide nanoparticles using prickly pear peel fruit extract: characterization and catalytic activity. *Inorganic Chemistry Communications*, 134.

Bayda, S., Adeel, M., Tuccinardi, T., Cordani, M. and Rizzolio, F., 2020. The history of nanoscience and nanotechnology: from chemical–physical applications to nanomedicine. *Molecules*, 25 (1), pp. 112.

Buazar, F., Sweidi, S., Badri M. and Kroushawi, F., 2019. Biofabrication of highly pure copper oxide nanoparticles using wheat seed extract and their catalytic activity: a mechanistic approach. *Green Processing and Synthesis*, 8 (1), pp. 691-702.

Burkart, A., Aasen, H., Alonso, L. and Menz, 2015. Angular dependency of hyperspectral measurements over wheat characterized by a novel UAV based goniometer. *Remote Sensing*, 7 (1), pp. 725-746.

Chai, H.Y., Lam, S.M. and Sin, J.C., 2019. Green synthesis of ZnO nanoparticles using *Hibiscus rosa-sinensis* leaves extracts and evaluation of their photocatalytic activities. *AIP Conference Proceedings*, 2157 (1).

Charles, A. and Cheng, C.K., 2018. Recent advances in photocatalytic treatment of palm oil mill effluent (POME): a review. *International Journal of Engineering & Technology*, 7 (4.34), pp. 389-393.

Cheng, Y.W., Chang, Y.S., Ng, K.H., Wu, T.Y. and Cheng, C.K., 2021. Photocatalytic restoration of liquid effluent from oil palm agroindustry in Malaysia using tungsten oxides catalyst. *Journal of Cleaner Production*, 162, pp. 205-219.

Dashti, A.F., Aziz, H.A., Ibrahim, H.A. and Zahed, M.A., 2020. Suspended solid removal of palm oil mill effluent using horizontal roughing filter and calcinated limestone. *Water Air Soil Pollut*, 231 (8), pp. 393.

Das, P., Ghosh, S., Dam, S. and Baskey, M., 2018. *Madhuca longifolia* plant mediated green synthesis of cupric oxide nanoparticles: A promising environmentally sustainable material for waste water treatment and efficient antibacterial agent. *Journal of Photochemistry and Photobiology B: Biology*, 189, pp. 66-73.

Dehbi, F. et al., 2013. Bioactive constituents, antioxidant activity and *in vitro* cancer cell cytotoxicity of Moroccan prickly pear (*Opuntia ficus indica L*.) juices. *Journal of Natural Sciences Research*, 3 (14), pp. 12-20.

Dev, C. and Nidhi, S.R.R.S., 2016. Basketful benefit of *Citrus limon*. *International Research Journal of Pharmacy*, 7 (6), pp. 1-4.

Felix, S., Chakkravarthy, R.B.P. and Grace, A.N., 2015. Microwave assisted synthesis of copper oxide and its application in electrochemical sensing. *International Conference on Materials Science and Technology*, 73 (1).

Feugang, J.M., 2017. Novel agents for sperm purification, sorting, and imaging. *Molecular Reproduction and Development*, 84 (9), pp. 1-10.

Ganapuram, B.R. et al., 2015. Catalytic reduction of methylene blue and congo red dyes using green synthesized gold nanoparticles capped by *Salmalia malabarica* gum. *International Nano Letters*, 5, pp. 215–222.

Ghidan, A.Y. and Antary, T.M.A., 2019. Applications of nanotechnology in agriculture. In: Stoytcheva, M and Zlatev, R. (eds.). *Applications of Nanobiotechnology*. London: IntechOpen.

Grigore, M.E., Biscu, E.R., Holban, A.M., Gestal, M.C. and Grumezescu, A.H., 2016. Methods of synthesis, properties and biomedical applications of CuO nanoparticles. *Pharmaceuticals*, 9 (4), pp. 75.

Harrison, E., Smith, H. and Dekker, I., 2021. Designing & facilitating a bioeconomy in the capital regional district learning through the lenses of biomimicry, industrial symbiosis, and green chemistry. *Technical Report*.

Hulla, J., Sahu, S. and Hayes, A., 2015. Nanotechnology: history and future. *Human & Experimental Toxicology*, 34 (12), pp. 1318-1321.

Iravani, S., 2011. Green synthesis of metal nanoparticles using plants. *Green Chem*istry, 13, pp. 2638–2650.

Iwuagwu, J.O. and Ugwuanyi, J.O., 2014. Treatment and valorization of palm oil mill effluent through production of food grade yeast biomass. *Journal of Waste Management*, 2014 (1), pp 1-9.

Izah, S.C., 2016. Possible challenges of potential drivers of oil palm processing sector in Nigeria. *Journal of Biotechnology Research*, 2 (10), pp. 73-79.

Javed, R. et al., 2020. Role of capping agents in the application of nanoparticles in biomedicine and environmental remediation: recent trends and future prospects. *Journal of Nanobiotechnology*, 18 (172).

Kannan, K. et al., 2020. Facile fabrication of CuO nanoparticles via microwave-assisted method: photocatalytic, antimicrobial and anticancer enhancing performance. *International Journal of Environmental Analytical Chemistry*, 102 (5), pp. 1095-1108.

Khairy, L., Yang, T. and Saadoon, F., 2015. Study on color and antioxidant properties of rambutan seed fat as cocoa butter alternative. *International Journal on Advanced Science Engineering and Information Technology*, 5 (2), pp. 90-94.

Khan, I., Saeed, K. and Khan, I., 2019. Nanoparticles: properties, applications and toxicities. *Arabian Journal of Chemistry*, 12 (7), pp. 908-931.

Klimek-Szczykutowicz, M., Szopa, A. and Ekiert, H., 2020. *Citrus limon* (lemon) phenomenon-a review of the chemistry, pharmacological properties, applications in the modern pharmaceutical, food, and cosmetics industries, and biotechnological studies. *Plants*, 9 (1), pp. 119.

Komakech, R., Kim, Y., Matsabisa, G.M. and Kang, Y., 2019. Anti-inflammatory and analgesic potential of *Tamarindus indica* Linn. (Fabaceae): a narrative review. *Integrative Medicine Research*, 8 (3), pp. 181-186.

Koshy, J. and George, K.C., 2015. Annealing effects on crystallite size and band gap of CuO nanoparticles. *International Journal of NanoScience and Nanotechnology*, 6 (1), pp. 1-8.

Krishnaswamy, S., Ragupathi, V., Raman, S. and Ngarajan, G.S., 2019. Study of optical and electrical property of NaI-doped PPy thin film with excellent photocatalytic property at visible light. *Polymer Bulletin*, 76(4), pp. 5213–5231.

Mamade, A.M.G.N., Coelho, C.C.S., Freitas-Silva, O., Barboza, H.T.G. and Soares, A.G., 2020. Nutritional composition and antioxidant properties of fruits and vegetables. *Academic Press*, pp. 377-392.

Mansoori, G.A. and Soelaiman, T.A.F., 2005. Nanotechnology- an introduction for the standards community. *Journal of ASTM International*, 2(6), pp. 1-21.

Manyasree, D., Peddi, K.M. and Ravikumar, K., 2017. CuO nanoparticles: synthesis, characterization and their bactericidal efficacy. *International Journal of Applied Pharmaceutics*, 9 (6), pp. 71-74.

Martinez, G. et al., 2021. Environmental impact of nanoparticles, application as an emerging technology: a review. *Materials*, 14 (1), pp. 166.

Mohammad, S., Baidurah, S., Kobayashi, T., Ismail., N. and Leh, C.P., 2021. Palm oil mill effluent treatment processes- a review. *Processes*, 9 (5), pp. 739.

Ohring, M., 1995. Structure of solids. *Engineering Materials Science*, pp. 134.

Patel, G.M., Bhatt., G.J. and Deota, P.T., 2022. Synthesis and characterization of silicon-based hybrid nanoparticles. *Micro and Nano Technologies*, pp. 11-43.

Phang, Y.K. et al., 2021. Green synthesis and characterization of CuO nanoparticles derived from papaya peel extract for the photocatalytic degradation of palm oil mill effluent (POME). *Sustainability*, 13, pp. 796.

Radhakrisknan, A.A. and Beena, B.B., 2014. Structural and optical absorption analysis of CuO nanoparticles. *Indian Journal of Advances in Chemical Science*, 2 (2), pp. 158-161.

Ragunath, L. et al., 2021. Synthesis and characterization of copper oxide nanoparticles using rambutan peel extract via greener route. *Rasayan Joornal of Chem*istry, 14 (4), pp. 2660-2665.

Rajgovind, Sharma, G., Kr, D.P. Jasuja, N.D. and Joshi, S.C., 2015. *Pterocarpus marsupium* derived phyto-synthesis of copper oxide nanoparticles and their antimicrobial activities. *Microbial & Biochemical Technology*, 7 (3), pp. 140-144.

Rawat, R.S., 2015. Dense plasma focus - from alternative fusion source to versatile high energy density plasma source for plasma nanotechnology. *Journal of Physics Conference Series*, 591 (1).

Roguai, S. and Djelloul, A., 2021. A simple synthesis of CuO NPs for photocatalytic applications and theirs structural and optical properties. *Journal of New Technology and Materials*, 11 (2), pp. 53-57.

Sabanovic, E., Memic, M., Sulejmanovic, J. and Selovic, A., 2020. Simultaneous adsorption of heavy metals from water by novel lemon-peel based biomaterial. *Polish Journal of Chemical Technology*, 22 (1), pp. 46-53.

Sagir, M., Tahir, M.B., Akram, J., Tahir, M.S. and Waheed, U., 2020. Nanoparticles and significance of photocatalytic nanoparticles in wastewater treatment: a review. *Current Analytical Chemistry*, 16 (1), pp. 38-41.

Saha, P., Mahiuddin, M., Saha, N.K., Islam, A.B.M.N. and Ara, M.H., 2018. Investigation on fatty acid composition of oil extracted from *Carica papaya* L. Seed. *International Journal of Innovative Research in Science, Engineering and Technology*, 7 (10), pp. 10543-10548.

Saputera, W.H., Amri, A.F., Daiyan, R. and Sasongko, D., 2021. Photocatalytic technology for palm oil mill effluent (POME) wastewater treatment: current progress and future perspective. *Materials*, 14 (11), pp. 2846.

Saputera, W.H. et al., 2021. Photocatalytic degradation of palm oil mill effluent (POME) waste using $BiVO_4$ based catalysts. *Molecules*, 26 (20), pp. 6225.

Satishhkumar, A.S., Balasubramanian, K.A. and Ramkumar, T., 2020. Structural characterization of ZnO, CuO and Fe_2O_3 nanoparticles: evaluation of rietveld refinement. *Tierärztliche Praxis*, 40, pp. 1139-1154.

Sharma R.K, Goyal A.K and Bhat R.A., 2013. Antifertility activity of plants extracts on female reproduction: a review. *International Journal of Pharmacy and Biological Sciences*, 3 (3), pp. 493-514.

Sharma, S. and Kumar, K., 2020. Aloe-vera leaf extract as a green agent for the synthesis of CuO nanoparticles inactivating bacteria pathogens and dye. *Journal of Dispersion Science and Technology*, 42 (13), pp. 1-13.

Singh, J. et al., 2018. 'Green' synthesis of metals and their oxide nanoparticles: applications for environmental remediation. J*ournal of Nanobiotechnology*, 16 (1), pp. 84.

Sukumar, S., Rudrasenan, A. and Nambiar, D.P., 2020. Green-synthesized rice-shaped copper oxide nanoparticles using *Caesalpinia bonducella* seed extract and their applications. *ACS Omega*, 5 (2), pp. 1040-1051.

Thamer, N.A., Muftin, N.Q. and Al-Rubae, S.H.N., 2018. Optimization properties and characterization of green synthesis of copper oxide nanoparticles using aqueous extract of *Cordia myxa* L. leaves. *Asian Journal of Chemistry*, 30 (7), pp. 1559-1563.

Ullah, H., Ullah, Z., Fazal, A. and Irfan, M., 2017. Use of vegetable waste extracts for controlling microstructure of CuO nanoparticles: green synthesis, characterization, and photocatalytic applications. *Journal of Chemistry*, 2017 (1), pp. 1-5.

Varadavenkatesan, T., Pai, S., Vinayagam, R. and Selvaraj, R., 2021. Characterization of silver nano-spheres synthesized using the extract of *Arachis hypogaea* nuts and their catalytic potential to degrade dyes. *Materials Chemistry and Physics*, 272 (60).

Veisi, H. et al., 2021. Biosynthesis of CuO nanoparticles using aqueous extract of herbal tea (*Stachys Lavandulifolia*) flowers and evaluation of its catalytic activity. *Scientific Reports*, 11 (1).

Zainuri, N.Z. et al., 2018. Palm oil mill secondary effluent (POMSE) treatment via photocatalysis process in the present of Zno-PEG nanoparticles. *Journal of Water Process Engineering*, 26, pp 10-16.

Zaman, M., Poolla, R., Singh, P. and Gudipati, T., 2020. Biogenic synthesis of CuO nanoparticles using *Tamarindus indica* L. and a study of their photocatalytic and antibacterial activity. *Environmental Nanotechnology. Monitoring & Management*, 14 (14).

APPENDICES

Appendix A

Calculation of crystalline size by using Debye-Scherrer equation

To calculate β

$$\beta = \frac{FWHM\ in\ 2\theta\ x\ \pi}{180°}$$

$$= \frac{0.35690\ x\ \pi}{180°}$$

$$= 6.2291 \text{ x } 10^{-3}$$

Debye-Scherrer Equation

$$D = \frac{k\lambda}{\beta \cos\theta}$$

$$= \frac{0.9\ x\ 1.5406\ x\ 10^{-10}}{6.2291 \text{ x } 10^{-3} \cos 17.74°}$$

$$= \frac{1.38654\ x\ 10^{-10}}{5.9329 \text{ x } 10^{-3}}$$

$$= 2.337 \text{ x } 10^{-8} \text{ m}$$

$$= 23.37 \text{ nm}$$

where

D = Mean size of nanoparticle

k = Scherrer constant, 0.9

λ = Wavelength of the X-ray source, (Cu, K_α radiation = 1.5406 x 10^{-10} m)

β = Width of diffraction broadening at full-width half maximum (in radian 2θ)

θ = Bragg's diffraction angle

Appendix B

*** Basic Data Process ***

Group : Standard
Data : TLX_CuONPs_L

Strongest 3 peaks

no.	peak no.	2Theta (deg)	d (A)	I/I1	FWHM (deg)	Intensity (Counts)	Integrated Int (Counts)
1	4	35.4808	2.52802	100	0.35690	11799	238634
2	5	38.7118	2.32414	97	0.40940	11458	283933
3	7	48.7424	1.86673	25	0.37280	3008	73826

Peak Data List

peak no.	2Theta (deg)	d (A)	I/I1	FWHM (deg)	Intensity (Counts)	Integrated Int (Counts)
1	31.9509	2.79880	21	0.31640	2429	41893
2	32.4800	2.75440	11	0.29420	1241	23533
3	34.8200	2.57447	22	0.35220	2544	56611
4	35.4808	2.52802	100	0.35690	11799	238634
5	38.7118	2.32414	97	0.40940	11458	283933
6	43.7487	2.06752	6	0.30320	687	13666
7	48.7424	1.86673	25	0.37280	3008	73826
8	53.4400	1.71318	6	0.48260	747	24718
9	55.0173	1.66774	4	0.24420	481	7286
10	58.2714	1.58212	12	0.41340	1392	36218
11	59.1600	1.56045	3	0.24600	376	8298
12	60.6970	1.52457	3	0.40600	400	10685
13	61.5310	1.50589	18	0.34820	2173	38051
14	61.8800	1.49823	3	0.20240	384	7513
15	65.8200	1.41776	10	0.58660	1129	35403
16	66.2400	1.40979	15	0.46820	1758	33115
17	66.7600	1.40006	3	0.36000	374	10342
18	67.5600	1.38542	4	0.26060	441	7925
19	68.0166	1.37723	15	0.49610	1759	44999
20	72.3941	1.30435	6	0.38310	660	17591
21	75.1095	1.26378	8	0.56250	914	29552

Figure: XRD information of synthesized CuO NPs (Part I)

Appendix C

```
          ***  Basic Data Process  ***

# Data Infomation
          Group                : Standard
          Data                 : TLX_CuONPs_L
          Sample Nmae          : CuONPs_L
          Comment              :
          Date & Time          : 10-12-21 16:28:18

# Measurement Condition
    X-ray tube
          target               : Cu
          voltage              : 40.0 (kV)
          current              : 30.0 (mA)
    Slits
          Auto Slit            : not Used
          divergence slit      :   1.00000 (deg)
          scatter slit         :   1.00000 (deg)
          receiving slit       :   0.30000(mm)
    Scanning
          drive axis           : Theta-2Theta
          scan range           :   10.0000 - 80.0000 (deg)
          scan mode            : Continuous Scan
          scan speed           :    2.0000 (deg/min)
          sampling pitch       :    0.0200 (deg)
          preset time          :    0.60 (sec)

# Data Process Condition
    Smoothing                  [ AUTO ]
          smoothing points     : 19
    B.G.Subtruction            [ AUTO ]
          sampling points      : 21
          repeat times         : 30
    Ka1-a2 Separate            [ MANUAL ]
          Ka1 a2 ratio         : 50 (%)
    Peak Search                [ AUTO ]
          differential points  : 19
          FWHM threhold        : 0.050 (deg)
          intensity threhold   : 30 (par mil)
          FWHM ratio  (n-1)/n  : 2
    System error Correction    [ NO ]
    Precise peak Correction    [ NO ]
```

Figure: XRD information of synthesized CuO NPs (Part II)

Appendix D

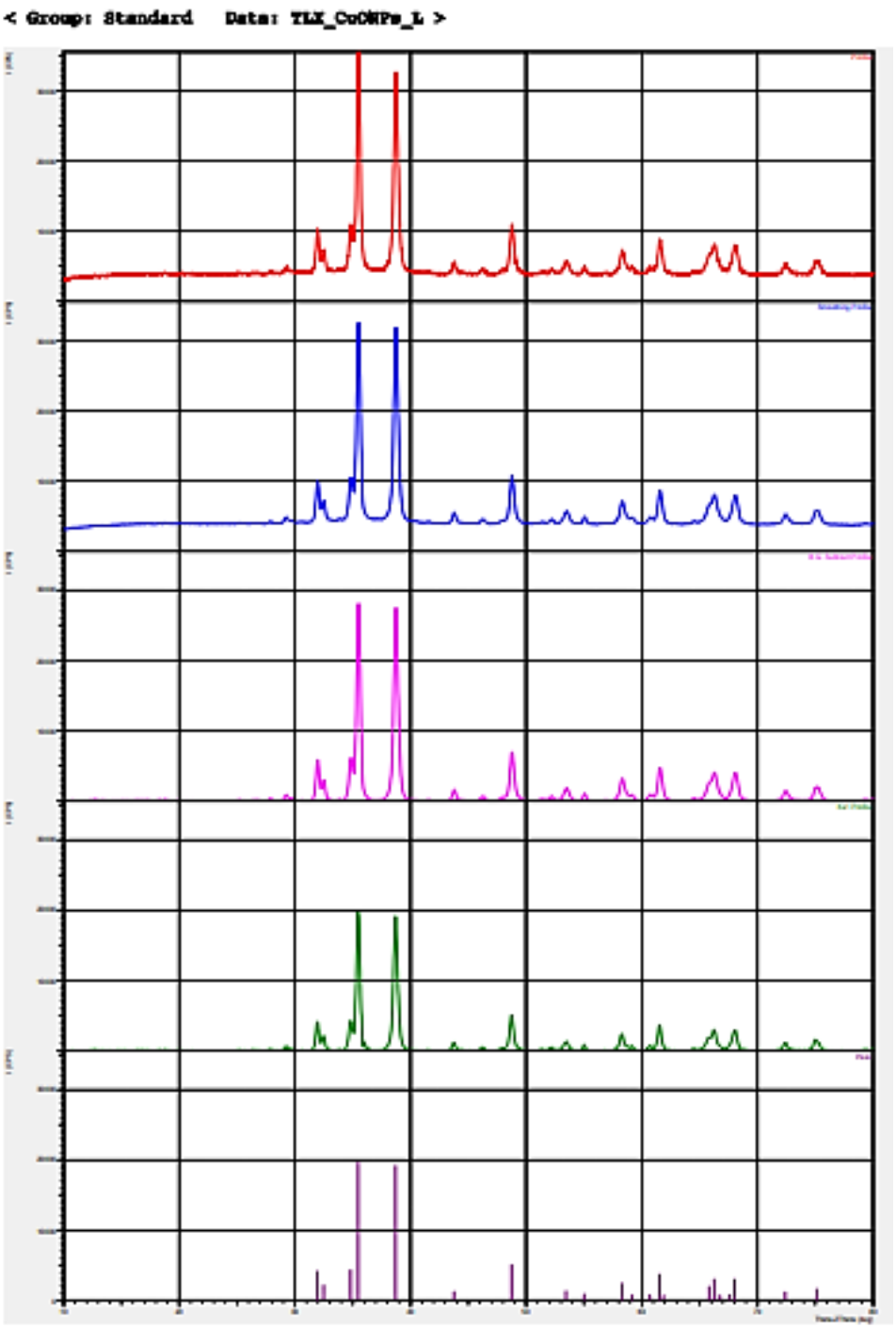

Figure: XRD information of synthesized CuO NPs (Part III)

Appendix E

Match! Phase Analysis Report

Universiti Tunku Abdul Rahman, Faculty of Science

Sample: CuONPs_L ()

Sample Data	
File name	TLX_CuONPs_L.RAW
File path	C:/xddat/Standard/TLX_CuONPs_L
Data collected	Oct 12, 2021 17:05:14
Data range	10.180° - 80.180°
Original data range	10.000° - 80.000°
Number of points	3501
Step size	0.020
Rietveld refinement converged	No
Alpha2 subtracted	No
Background subtr.	No
Data smoothed	No
2theta correction	0.18°
Radiation	X-rays
Wavelength	1.540600 Å

Matched Phases

Index	*Amount (%)*	*Name*	*Formula sum*
A	93.3	Copper Oxide Tenorite, syn	Cu O
	6.7	*Unidentified peak area*	

A: Copper Oxide Tenorite, syn (93.3 %)	
Formula sum	Cu O
Entry number	01-089-5896
Figure-of-Merit (FoM)	0.923938
Total number of peaks	71
Peaks in range	23
Peaks matched	16
Intensity scale factor	0.80
Space group	C2/c
Crystal system	monoclinic
Unit cell	a= 4.6830 Å b= 3.4240 Å c= 5.1290 Å β= 99.440 °
I/Ic	3.76
Calc. density	6.513 g/cm³
Reference	Massarotti, V., Capsoni, D., Bini, M., Altomare, A., Moliterni, A.G.G., Z. Kristallogr. **213**, 259 (1998)

Candidates

Name	*Formula*	*Entry No.*	*FoM*
Copper Vanadium Oxide	Cu V2 O5	00-043-0080	0.7786
Copper Vanadium Fluoride Oxide	Cu V2 F O4	00-043-0082	0.7364
Copper Strontium Yttrium Oxide	Cu4 Sr4 Y3 O14	00-048-0658	0.7103
Copper Strontium Yttrium Oxide	Cu2 Sr2 Y1.5 O7	00-048-0752	0.7103
Copper Oxide (Paramelaconite, syn)	Cu4 O3	01-071-6397	0.6912
Strontium Europium Copper Oxide	(Sr0.79 Eu0.21) Cu O1.94	01-070-7225	0.6901
Copper Strontium Cobalt Holmium Oxide	Ho2 Sr Cu0.6 Co1.4 O6.5	00-048-0250	0.6887
Copper Strontium Cobalt Yttrium Oxide	Y2 Sr Cu0.6 Co1.4 O6.5	00-048-0248	0.6867
Copper Oxide (Paramelaconite)	Cu16 O14.15	01-071-0251	0.6839
Bismuth Lead Lanthanum Strontium Copper Oxide	(Bi0.1 Pb0.1 La Sr0.8) (Pb0.3 La0.2 Sr0.5) Cu2 O5.45	01-088-1018	0.6823
Cobalt Copper Strontium Yttrium Oxide	Y2 Sr (Cu0.6 Co1.4) O6.5	01-083-9730	0.6748
Yttrium Strontium Copper Cobalt Oxide	Y2 Sr Cu0.6 Co1.4 O6.5	01-089-8354	0.6741
Lead Lanthanum Strontium Copper Oxide	(Pb0.4 Sr0.6) (Pb0.1 La1.4 Sr0.5) Cu2 O5.26	01-086-0504	0.6679
Copper Strontium Ruthenium Oxide	Sr (Ru0.8 Cu0.2) O3	01-077-8646	0.6675
Copper Strontium Manganese Oxide	Sr3.95 Mn2 Cu O9	00-056-0381	0.6602
Strontium Praseodymium Copper Oxide	(Sr0.9 Pr0.1) Cu O2	01-087-1315	0.6595
Copper Lead Strontium Praseodymium Oxide	Cu2.4 Pb0.522 Sr2 Pr O6.53	00-048-0143	0.6558
Mercury Molybdenum Strontium Lanthanum Copper Oxide	(Hg0.62 Mo0.38) Sr2 (Sr0.45 La0.55) Cu2 O6.93	01-089-8210	0.6534
Lead Lanthanum Strontium Copper Oxide	(Pb0.05 La0.70 Sr0.25)2 (Pb0.40 Sr0.60) Cu2 O5.726	01-087-1506	0.6518
Lead Strontium Praseodymium Copper Oxide	(Pb0.522 Cu0.4) Sr2 Pr Cu2 O6.53	01-085-1941	0.6516
Barium Copper Strontium Cerium Gadolinium Titanium Oxide	Ti3 Ba2 Sr Gd2.25 Ce0.75 Cu2 O16	00-050-0431	0.6498
Barium Copper Yttrium Oxide	Ba2 Y Cu3 O6	01-079-0503	0.6491
Yttrium Barium Copper Oxide	Y Ba2 Cu3 O6	01-081-0889	0.6486
Yttrium Barium Copper Oxide	Y Ba2 Cu3 O6	01-088-0442	0.6473
Lanthanum Strontium Copper Titanium Oxide	La2 Sr4 Cu2 Ti2 O13.4	01-087-1180	0.6450
Copper Oxide (Paramelaconite, syn)	Cu2 +1 Cu2 +2 O3	00-049-1830	0.6445
Mercury Vanadium Strontium Calcium Neodymium Copper Oxide	(Hg0.61 V0.39) Sr2 (Ca0.41 Nd0.59) Cu2 O6.78	01-088-0081	0.6411

Figure: XRD information of synthesized CuO NPs, ICDD card No. 01-089-5896 (Part I)

Appendix F

Yttrium Barium Copper Oxide	Y Ba2 Cu3 O6.03	01-087-1361	0.6405
Yttrium Barium Copper Oxide	Y Ba2 Cu3 O6	01-080-0264	0.6402
Barium Calcium Copper Yttrium Oxide	(Y0.85 Ca0.15) Ba2 Cu3 O6	01-084-2085	0.6400
Copper Iron Titanium Oxide	Cu1.4 Ti0.4 Fe1.2 O4	00-057-0064	0.6386
Copper Strontium Lanthanum Oxide	La2 Sr Cu2 O6	00-045-0011	0.6384
Copper Strontium Gallium Yttrium Cerium Oxide	Ga Sr2 (Y , Ce)2 Cu2 O9	00-048-0253	0.6381
Copper Strontium Neodymium Oxide	Sr0.86 Nd0.14 Cu O2	00-049-0637	0.6366
Copper Iron Oxide (Delafossite)	Cu2 Fe2 O4	00-003-0870	0.6345
Copper Platinum Iron Oxide	Cu0.95 Pt0.05 Fe O2	00-063-0274	0.6342
Copper Lead Strontium Neodymium Oxide	(Pb , Cu) (Sr , Nd)2 Nd Cu2 O7-x	00-053-1170	0.6338
Yttrium Barium Copper Oxide	Y Ba2 Cu3 O6	01-080-0494	0.6337
Yttrium Barium Copper Oxide	Y Ba2 Cu3 O6	01-079-1808	0.6324
Mercury Lead Strontium Lanthanum Copper Oxide	(Hg0.28 Pb0.5 Cu0.22) (Sr1.7 La0.3) (Sr0.44 La0.56) Cu2 O6.56	01-087-2339	0.6324
Copper Strontium Gallium Lanthanum Oxide	La Sr2 Ga Cu2 O7	00-045-0302	0.6310
Lanthanum Strontium Copper Oxide	La1.8 Sr1.2 Cu2 O5.86	01-077-0580	0.6307
Strontium Neodymium Copper Oxide	(Sr0.86 Nd0.14) Cu O2	01-085-1946	0.6296
Copper Iron Vanadium Oxide	Cu (Fe0.75 V0.25) O2	01-074-3355	0.6294
Lanthanum Strontium Copper Oxide	(La2 Sr) Cu2 O6.03	01-089-8784	0.6273
Lanthanum Barium Strontium Copper Oxide	(La1.9 Ba0.1 Sr) Cu2 O6.30	01-080-1368	0.6258
Copper Strontium Neodymium Oxide	(Sr0.83 Nd0.17) Cu O2	00-051-0308	0.6250
Copper Iron Nickel Zinc Oxide	Cu0.3 Fe1.7 Ni0.65 Zn0.35 O4	00-048-0490	0.6242
Copper Strontium Cobalt Terbium Oxide	Tb2 Sr Co1.4 Cu0.6 O6.5	00-049-0313	0.6240
Lead Strontium Barium Yttrium Calcium Copper Oxide	Pb0.8 Sr1.2 Ba Y0.7 Ca0.3 Cu3 O6.8	01-081-0064	0.6235
Lanthanum Strontium Copper Oxide	La2 Sr Cu2 O6.03	01-088-1601	0.6227
Copper Mercury Strontium Cerium Yttrium Oxide	Hg0.06 Cu2.89 Ce0.39 Sr1.70 Y1.96 O8.63	00-050-0118	0.6222
and 47 others...			

Search-Match

Settings

Reference database used	PDF-2 Release 2016 RDB
Automatic zeropoint adaptation	Yes
Minimum figure-of-merit (FoM)	0.60
2theta window for peak corr.	0.30 deg.
Minimum rel. int. for peak corr.	1
Parameter/influence 2theta	0.50
Parameter/influence intensities	0.50
Parameter multiple/single phase(s)	0.50

Selection Criteria

Elements:

Elements that must be present:	O, Cu
Elements that may be present:	All elements not mentioned above

Peak List

No.	*2theta [°]*	*d [Å]*	*I/I0*	*FWHM*	*Matched*
1	29.46	3.0291	26.97	0.2400	
2	32.15	2.7817	195.69	0.2800	
3	32.69	2.7373	100.05	0.2800	A
4	35.04	2.5591	202.32	0.4000	
5	35.69	2.5133	1000.00	0.3200	A
6	38.92	2.3124	908.45	0.4000	A
7	43.97	2.0577	49.72	0.2800	
8	48.95	1.8592	224.42	0.4000	A
9	53.62	1.7079	50.07	0.4800	A
10	55.22	1.6620	32.62	0.2400	
11	58.42	1.5784	92.19	0.3600	A
12	61.74	1.5013	152.76	0.4000	A
13	65.94	1.4155	67.43	0.4800	A
14	66.44	1.4060	120.68	0.5600	A
15	68.20	1.3740	115.23	0.4400	A
16	68.52	1.3683	65.82	0.2800	
17	75.14	1.2633	50.96	0.2800	A
18	75.42	1.2593	60.87	0.4400	A

Rietveld Refinement using FullProf

Calculation was not run or did not converge.

Crystallite Size Estimation using Scherrer Formula

Calculation was not run.

Degree of crystallinity analysis

Figure: XRD information of synthesized CuO NPs, ICDD card No.01-089-5896 (Part II)

Appendix G

Profile area	*Counts*	*Amount*
Total area	9815672	100.00%
Diffraction peaks	1581839	16.12%
Background	8233833	83.88%
Instrumental background	892103	9.09%
Amorphous phases	7341730	74.80%

Degree of crystallinity (DOC) = 17.73%
Amorphous content (weight %) =82.27%

Integrated Profile Areas

Based on calculated profile

Profile area	*Counts*	*Amount*
Overall diffraction profile	9815672	100.00%
Background radiation	8233833	83.88%
Diffraction peaks	1581839	16.12%
Peak area belonging to selected phases	923882	9.41%
Peak area of phase A (Copper Oxide Tenorite, syn)	*923882*	*9.41%*
Unidentified peak area	657956	6.70%

Peak Residuals

Peak data	*Counts*	*Amount*
Overall peak intensity	31242	100.00%
Peak intensity belonging to selected phases	28341	90.71%
Unidentified peak intensity	2901	9.29%

Diffraction Pattern Graphics

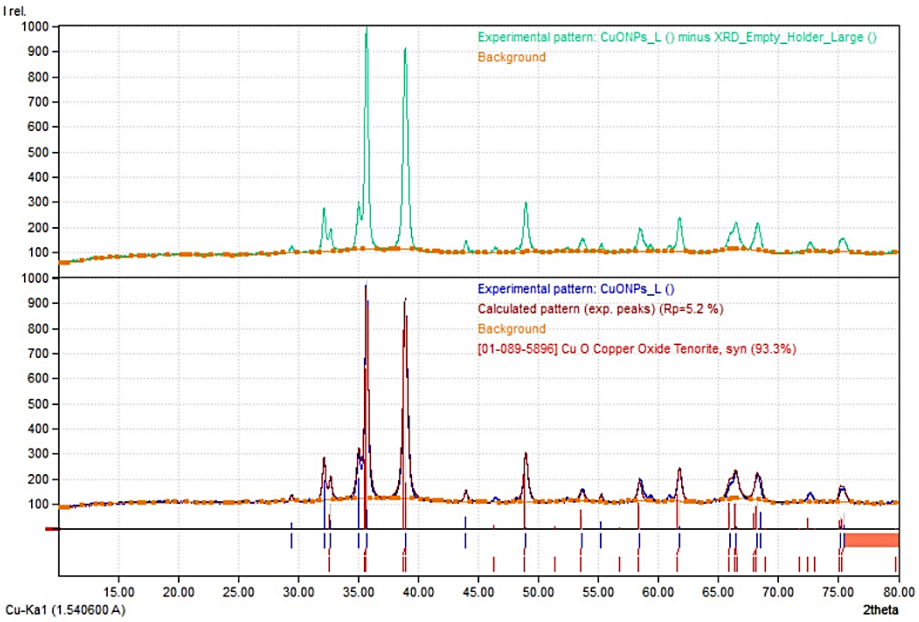

PDF Database Copyright International Centre for Diffraction Data (ICDD)
Match! Copyright © 2003-2018 CRYSTAL IMPACT, Bonn, Germany

Figure: XRD information of synthesized CuO NPs, ICDD card No.01-089-5896 (Part III)

Appendix H

Project: Project 1 Owner: INCA Site: Site of Interest 3	Sample: Sample 1 Type: Default ID: TLX CuO

Spectrum Label: Spectrum 1

Livetime 15.0 s

Acquisition geometry (degrees):
Tilt = 0.0
Azimuth = 0.0
Elevation = 29.0

Accelerating voltage = 20.00 kV

Total spectrum counts = 111880

Sample data :	Energy (eV)	Resn. (eV)	Area
Strobe :	7.5	57.38	248872

Optimization data : Cobalt ...

	Energy (eV)	Resn. (eV)	Area
Strobe :	.0	47.71	247540
Optimization element :	6922.0	138.74	83263

Sample is unpolished X-ray corrections may be approximate.
Sample is coated with Platinum - thickness (nm): 15.0, density (g/cm3): 21.45
Thresholding has been selected : All quantitative results below 2 sigma have been set to zero
Detector efficiency : Read from file (X-Max 2.efy)
Pulse pile up correction performed.

Spectrum processing :
No peaks omitted

Processing option : All elements analyzed (Normalised)
Number of iterations = 3

Standard :
O SiO2 1-Jun-1999 12:00 AM
K MAD-10 Feldspar 1-Jun-1999 12:00 AM
Cu Cu 1-Jun-1999 12:00 AM

Element	App Conc.	Intensity Corrn.	Weight%	Weight% Sigma	Atomic%
O K	6.16	0.4521	18.14	0.53	46.02
K K	3.00	0.9417	4.25	0.13	4.41
Cu K	54.17	0.9299	77.61	0.52	49.58
Totals			100.00		

Figure: EDX information of synthesized CuO NPs

Appendix I

Percentage of COD removal = $\frac{COD_0 - COD_t}{COD_0}$

where

COD_0 = Initial COD value of the POME before expose to UV irradiation (mg/L)

COD_t = COD value of the POME after photodegradation at different time interval (mg/L)

Table: Photocatalytic degradation of POME by CuO NPs as a function of contact time under UV irradiation

Contact time (min)	COD_t	COD_t / COD_0
0	107	1
30	58	0.54
60	41	0.38
90	34	0.32
120	28	0.26
150	24	0.22
180	20	0.19

Appendix J

Table: Degradation of POME by CuO NPs as a function of contact time in dark condition

Contact time (min)	COD_t	COD_t / COD_0
0	107	1
30	58	1
60	41	1
90	34	0.98
120	28	0.96
150	24	0.94
180	20	0.90

Appendix K

Table: Degradation of POME as a function of contact time without the addition of CuO NPs under UV irradiation

Contact time (min)	COD_t	COD_t / COD_0
0	107	1
30	58	0.98
60	41	0.96
90	34	0.94
120	28	0.92
150	24	0.88
180	20	0.84

Appendix L

Phytotoxicity = $\frac{L_c - L_s}{L_c} \; x \; 100\%$

where

L_c = Radicle length of control

L_s = Radicle length of samples

Table: Phytotoxicity of POME on *Vigna radiate L.*

Solution	Radicle length (cm)	Phytotoxicity (%)
Tap water	12.0	0
POME before photodegradation	3.5	70.8
POME after photodegradation	11.0	8.3